ECMWF COPERNICUS REPORT

Copernicus Climate Change Service

Product Quality Assessment Report (PQAR)

Global L4 Sea and Sea-Ice Surface Temperature (SST/IST) Climate Data Record, Version 1.0

WP2-FDDP-SST/IST-v1.0

Issued by: Danish Meteorological Institute/ I. Karagali

Date: 23/04/2025

Ref: C3S2_312b_WP2-FDDP-SST/IST_202501_PQAR_v1.1

Official reference number service contract: 2022/C3S2_312b_MOi/SC1

PROGRAMME OF THE EUROPEAN UNION

IMPLEMENTED BY ECMWF

Contributors

DANISH METEOROLOGICAL INSTITUTE
Ioanna Karagali
Pia Englyst
Ida Lundtorp Olsen
Guisella Gracitua

History of document modifications

Version	Date	Description of modification	Chapters / Sections
1.0	29/01/2025	First version	All
1.1	23/04/2025	Document amended in response to independent review.	All

List of datasets covered by this document

Deliverable ID	Product title	Product type (CDR, ICDR)	Version number	Delivery date
WP2-FDDP-SST-v1.0	SST/IST CDR L4	CDR	1.0	31/10/2024
WP2-ICDR-SST-v1.0	SST/IST ICDR L4	ICDR	1.0	31/10/2024

Related documents

Reference ID	Document
D1	Embury O., 2021 Sea Surface Temperature: Product Quality Assessment Report. Copernicus Climate Change Service. Document ref. D2.SST.1-v3.0_PQAR_of_v2.1SST_products_v5.1. https://dast.copernicus-climate.eu/documents/satellite-sea-surface-temperature/v2.1/D2.SST.2-v3.0_PQAR_of_v2.1SST_products_v5.1_APPROVED_Ver1.pdf
D2	Karagali, I. et al. (2024). Global L4 Sea and Sea Ice Surface Temperature Climate Data Records, Version 1.0: Product Quality Assurance Document. Copernicus Climate Change Service. Document ref. C3S2-312b_WP2-PDDP-SST/IST_2024_PQAD_v1.2.
D3	Karagali, I. et al. (2024). Global L4 Sea and Sea Ice Surface Temperature Climate Data Records, Version 1.0: Product User Guide and Specifications Document. Copernicus Climate Change Service. Document ref. C3S2-312b_WP2-FDDP-SST/IST_2024_PUGS_v1.1.
D4	Karagali, I. et al. (2024). Global L4 Sea and Sea Ice Surface Temperature Climate Data Records, Version 1.0: Algorithm Theoretical Basis Document. Copernicus Climate Change Service. Document ref. C3S2-312b_WP2-FDDP-SST/IST_2024_ATBD_v1.1.
D5	Karagali, I. et al. (2024). Global L4 Sea and Sea Ice Surface Temperature Climate Data Records, Version 1.0: Target Requirements and Gap Analysis Document. Copernicus Climate Change Service. Document ref. C3S2_312b_WP3-TRGAD_SST/IST_2024_v1.1.

Acronyms

Acronym	Definition
AMSR-E	Advanced Microwave Scanning Radiometer for the Earth Observing System
AMSR2	Advanced Microwave Scanning Radiometer 2
ATSR	Along Track Scanning Radiometer
ATBD	Algorithm Theoretical Basis Document
AVHRR	Advanced Very High Resolution Radiometer
AASTI	Arctic and Antarctic Ice Surface Temperatures from AVHRR
a.g.l.	Above ground level
CARRA2	Copernicus Arctic Regional Reanalysis 2nd generation
C3S	Copernicus Climate Change Service
CCI	Climate Change Initiative
CDR	Climate Data Record
CDS	Climate Data Store
CEDA	Centre for Environmental Data Analysis
CRREL	Cold Regions Research Engineering Laboratory
DMI	Danish Meteorological Institute
DMI-MSC-SIC	Danish Meteorological Institute's Multi-Sensor Composite of Sea Ice Concentration data
ECMWF	European Centre for Medium-Range Weather Forecasts
ESA	European Space Agency
EUMETSAT	European Meteorological Satellites
EPS	EUMETSAT Polar System
ERS	European Remote Sensing
EOCIS	UK Earth Observation Climate Information Service
FMI	Finnish Meteorological Institute
GAC	Global Area Coverage
GDS	GHRSST Data Specification
GCOM	Global Change Observation Mission
GHRSST	Group for High Resolution SST
ICDR	Interim Climate Data Record
TIR	Thermal Infrared
IST	Sea Ice Surface Temperature
JAXA	Japan Aerospace Exploration Agency
LECT	Local Equator Crossing Time
L2	Level-2 data product
L2P	Level-2 Pre-processed data product
L3	Level-3 data product
L3C	Level-3 Collated data product

L3U	Level-3 Uncollated data product
L4	Level-4 data product
MCAS	Marine and Climate Advisory Service
MIZ	Marginal Ice Zone
MetNo	Norwegian Meteorological Institute
NASA	National Aeronautics and Space Administration
NP	North Pole
NOAA	National Oceanographic and Atmospheric Administration
NWP	Numerical Weather Prediction
OSI SAF	Ocean and Sea Ice Satellite Application Facility
OI	Optimal Interpolation
OSTIA	Operational Sea Surface Temperature and Ice Analysis
PMW	Passive Microwave
POES	Polar Operational Environmental Satellites
RDAC	Regional Data Assembly Centre
R&D	Research and development
SI	Sea Ice
SIC	Sea-ice concentration
SIMB3	Seasonal Ice Mass Balance Buoy 3
SMHI	Swedish Meteorological and Hydrological Institute
SLSTR	Sea and Land Surface Temperature Radiometer
SST	Sea Surface Temperature
USNIC	U.S. National Ice Center
UISST	Under-ice SST
UWC-W	United Weather Centres West

General definitions

Climate Data Record (CDR) – Climate Data Record, defines a time series of measurements of sufficient length, consistency, and continuity to determine climate variability and change. Further satellite-based CDRs can be segmented into Fundamental CDRs (FCDRs), which are calibrated and quality-controlled sensor data that have been improved over time, and Thematic CDRs (TCDRs), which are geophysical variables derived from the FCDRs, such as sea surface temperature and cloud fraction.

Interim Climate Data Record (ICDR) – Interim Climate Data Record, defines a dataset that has been forward processed, using the baselined Climate Data Record algorithm and processing environment but whose consistency and continuity have not been verified. Eventually, it will be necessary to perform a new reprocessing of the CDR and ICDR parts together to guarantee consistency, and the new reprocessed data record will replace the old CDR.

Sea-ice concentration (SIC) – as fraction (percentage) of the sea surface area of the grid cell containing sea-ice.

Sea Surface Temperature (SST) – the temperature of the ocean water close to the surface.

SST_{20cm} – Sea Surface Temperature adjusted for the standard depth of 0.2 m and time representative of the daily mean, representative of the water temperature free, or almost free of any diurnal warming.

Sea Ice Surface Temperature (IST) – The surface temperature of ice or snow on sea ice, representative of the surface skin temperature over sea ice.

Open ocean – Corresponds to ice-free ocean or containing very little ice (<15 %), thus the surface temperature is classified as sea surface temperature (SST).

Sea Ice – Corresponds to ocean surface covered by sea ice (>70%) thus the surface temperature is classified as sea-ice surface temperature (IST).

Marginal Ice Zone (MIZ) – Marginal Ice Zone, a part of the seasonal ice zone that varies in width (100 to 200 kilometres) that extends from the ice edge into the ice pack, where waves and swells affect the ice; often characterized by highly variable ice conditions; in general, it is wider in the Antarctic than the Arctic.

Level-2 Pre processed (L2P) data product – Geophysical variables derived from Level 1 source data on the Level 1 grid (typically the satellite swath projection). Ancillary data and metadata added following GHRSST Data Specification.

Level-3 Uncollated (L3U) data product – L2 data granules remapped to a regular latitude/longitude grid without combining observations from multiple source files. L3U files will typically be “sparse”, corresponding to a single satellite orbit.

Level-3 Collated (L3C) data product – SST observations from a single instrument combined into a space-time grid. In this project, a typical L3C file may contain all the observations from a single instrument in a 24-hour period.

Level-3 Super-Collated (L3S) data product – SST observations from many instruments combined into a space-time grid. In this project, a typical L3S file may contain all the observations from all available instruments in a 24-hour period.

Level 4 (L4) data product – SST observations from multiple instruments using an analysis system (e.g. optimal interpolation) to produce a gridded, gap-free product

Goal (requirement) - The goal value is defined as an ideal requirement value, above which further improvements are not necessary.

Threshold (**requirement)** – The threshold value is defined as the minimum requirement value to be met to ensure that data are useful.

Accuracy - The closeness between the measured value and the reference (true) quantity value.

Stability - Trend in bias relative to constant reference measurements. 100% stability is associated with no trend over time.

Table of Contents

Scope of the document

This document is the Product Quality Assessment Report (PQAR) for the L4 Sea Surface and Sea-Ice Surface Temperature (SST/IST) Climate Data Record (CDR) and Interim CDR (ICDR) products, within the Copernicus Climate Change Service (C3S). This document builds upon the PQAR of the L4 SST CDR dataset v2.1 [D1] and summarizes the results of the validation for the replacement product which combines SST and IST as well as using the latest version (v3.0) of the ESA SST_cci input data. The assessment methodology is described in the C3S Product Quality Assurance Document [D2].

Executive summary

This document is the Product Quality Assessment Report (PQAR) for the L4 Sea Surface and Sea-Ice Surface Temperature (SST/IST) CDR/ICDR products. The C3S CDR covers the period 1982-2021 using ESA SST_cci v3.0 input SST data while the ICDR covers the period 2022-2024 and is intended to be used in combination with the corresponding SST CDR. Both ICDR and CDR datasets are generated using the same software and algorithms originally developed within the MyOcean project and currently applied to the operational Multi-Year products for the SST and IST delivered to the Copernicus Marine Service.
The CDR and ICDR were validated as a continuous dataset. The L4 SST and IST components and their uncertainties were assessed using a number of different in situ reference datasets (e.g. drifting buoys, moored buoys and Argo floats for the SST component and ice mass balance buoys, drifting ice stations and flight campaigns for the IST component). A multi-sensor matchup system (MMS) was used to compile the reference measurements and the corresponding SST/IST from the analyses. Robust statistics (median and robust standard deviation) were used when assessing differences between the reference data and the L4 SST/IST. Regarding the accuracy and stability for climate assessment, these are defined with respect to reference sensors (drifting buoys for the SST component and ice mass balance buoys and drifting ice stations for the IST component).

Concerning the SST component of the product:

- Median difference between SST values and the reference drifter data are -0.04 °C.
- Robust standard deviation: 0.28 °C (drifter data). Lower values are reported when using Argo floats (0.24 °C) and moored buoys (0.17 °C).
- The spatial distribution of the statistics shows that the product SST values are cooler than drifters at high latitudes and at the western-boundaries of continental shelves.
- Validation of the uncertainties provided with the L4 SST/IST dataset could only be performed for the SST component, supported by the availability of long-term reference measurements which have well characterised uncertainties. The analysis showed that the uncertainties calculated by the DMIOI algorithm are following the expected behaviour of increasing when the standard deviation between the L4 SST and reference in-situ observations increases.
- Spectral analysis of the SST component showed a high performance of the DMIOI scheme in terms of preserving the smaller scale features present in the high resolution input SST

observations. Spectral power decreased, following the theory for the mesoscale and the L4 SST/IST product maintains spectral power down to approximately twice its grid spacing.

Concerning the IST component of the product:

- Median differences with the Operation IceBridge flight data reporting surface skin measurements are 1.39 °C, while they range between -2.24 °C and -3.13 °C for buoys reporting 2-m air temperatures (depending on the buoy type).
- Robust standard deviation from the Operation IceBridge flight data is 2.52 °C, while it ranges from 3.24 °C to 3.38 °C for buoys reporting 2-m air temperatures (depending on the buoy type).
- The spatial distribution of the statistics shows that the product IST values are warmer than Operation IceBridge flight data and buoys reporting 2-m air temperature at high latitudes of the Northern Hemisphere, although small regions with large negative biases exist.
- Validation of the uncertainties provided with the L4 SST/IST dataset can not be performed for the IST component due to the lack of long-term reference measurements of skin temperature over the sea-ice. Instead, the assessment of the uncertainties was performed separately for the Marginal Ice Zone (MIZ) and fully sea-ice covered areas (IST) in terms of seasonal and annual variability. It was found that uncertainties for the MIZ are generally higher compared to the ones for IST. A seasonal cycle was also present in both along with a relatively stable performance of the uncertainties throughout the data record.

Climate assessment of the CDR and ICDR period (1982-2024) demonstrated the added benefit of combined SST/IST fields compared to only SST fields, as the trends estimated with the former are approximately 25-30% higher and comply with other findings on the Arctic amplification, i.e. that the Arctic has been warming by more than 4 times the global average (although no consensus has been reach on the exact figure).

Known issues are related to higher uncertainties in some of the sea ice concentration products, for some specific periods in time – mostly in the very early years, used to create the DMI-MSC-SIC field. The implication of this is that the Sea Ice Concentration field may be more uncertain for such areas in those dates.

This document is structured as follows. Section 1 gives an overview of the methodology used to validate the L4 SST/IST values, noting further information can be found in the Product Quality Assurance Document. Section 2 details the results of the different validation analyses, while Section 3 details a climatology assessment of trends and variability in the L4 SST/IST CDR and ICDR, performed relative to the 1991-2020 climatology. Finally, Section 4 details how the product relates to user requirements, taking into account the quality assessments detailed here.

1. Product validation methodology

This document applies to the L4 SST/IST CDR (1982-2021) and ICDR (2022-2023)[1] produced by C3S. These products are described in detail in the Product User Guide and Specification [D3] and Algorithm Theoretical Basis Document [D4]. For further details on the validation methodology see the Product Quality Assurance Document [D2].
Assessment of the product quality examined four aspects of the data products:

1. The SST and IST values,
2. The SST uncertainty, and IST uncertainty values,
3. The effective spatial resolution of the product by assessing spectra for the SST component,
4. The stability of the SST and IST CDR and ICDR records.

Match-up datasets containing coincident in situ observations and the satellite observations of the L4 SST/IST product were created for each type of reference observation and each component of the L4 product, separately.

1.1 Validation of SST

The SST reference dataset used to validate the CDR and ICDR SST component is comprised of in situ SST observations extracted from the Met Office Hadley Centre Integrated Ocean Dataset (HadIOD) v1.2.0.0 (Atkinson et al. 2014). Data are included for the following platform types:

1. Drifting buoys (extensively described in Section 2.1 of [D2]),
2. Global Tropical Moored Buoy Array (GTMBA, extensively described in Section 2.2 of [D2]),
3. Voluntary observing ships (extensively described in Section 2.3 of [D2]),
4. Argo floats (extensively described in Section 2.4 of [D2]).

1.2 Validation of IST

To validate the IST component of the CDR and ICDR, due to lack of in situ measurements of the ice surface temperature, a series of buoys and drifting stations were utilised, typically recording 2 meter air temperatures. Data have been acquired by:

- ECMWF distributed drifting ice buoys (1993–2015, extensively described in Section 2.5.1 of [D2]),
- US Army Cold Regions Research Engineering Laboratory (CRREL) mass balance buoys (2001-2017, extensively described in Section 2.5.2 of [D2]),
- Russian North Pole (NP) drifting ice stations (1982-1989, 2003-2012, extensively described in Section 2.5.3 of [D2]),
- Cryosphere Innovation Seasonal Ice Mass Balance Buoy 3 (SIMB3, extensively described in Section 2.5.3 of [D2]),

[1]The ICDR for 2024 has not been included in the validation due to unavailability of the entire ICDR and corresponding in-situ observations for 2024 at the time of writing.

- NASA IceBridge Flights. These include measurements from an on-board infra-red radiometer and thus are skin surface temperature measurements, and are extensively described in Section 2.6 of [D2].

1.3 Uncertainty validation

For SST, the uncertainty validation approach was similar to that performed by Alerskans et al. (2020) and Nielsen-Englyst et al. (2018, 2023). This approach is unfortunately not applicable for the IST validation results due to the lack of good quality in situ reference observations, that makes the spatial sampling component very large in comparisons between the L4 IST and the in situ measured near-surface air temperatures. However, using the SIMB3 stations, the modelled uncertainties of the IST component were assessed.

1.4 Spectral analysis

Due to the differences in Infra-Red (IR) and Passive MicroWave (PMW) footprint sizes and coverage, along with the Optimal Estimation method applied for gap-filling, it is important to assess the effective spatial resolution of the L4 SST/IST dataset. By the term effective spatial resolution it is meant the size of the true signal represented in the product compared to its grid spacing. For example, typical effective spatial resolutions of global SST datasets on a 0.05 degree grid can be as “low” as 60 km, i.e. the SST signals (eddies, etc) represented in the products are around 60 km, thus rendering the products very “smooth”.

A spectral analysis has been performed as part of the quality assessment. This involved the estimation of the power spectrum using the standard FFT method in the zonal direction (Thomson and Emery, 2014), noting that only open water points are included. The power spectrum per wave number was computed daily for each latitude band and averaged into bins for the years of investigation. Finally, a mean power spectrum is derived and this can be used to assess if the L4 SST/IST dataset is resolving SST signals of length-scales (size) similar to that of the product’s grid spacing, i.e. ~5-10 km. When assessing power spectra in the meso- and sub-mesoscale region, 200 km – 2 km, the theoretical −2 and −5/3 (−1.6) curves for the expected decrease of spectral power in the mesoscale to sub-mesoscale are also used to assess if the computed spectra follow the expected theory (see Vazquez-Cuervo et al., 2022, Castro et al., 2017).

1.5 Stability assessment

Based on the expected magnitude of a climate change signal (per decade), the requirements of an SST CDR are an accuracy of 0.1 °C and a stability (per decade) of 0.04 °C according to Ohring et al. (2005). For the Ice Surface temperature, which is also an ECV according to GCOS (since 2022), the CDR requirements are 0.3 °C/decade for the threshold stability and 0.1 °C/decade for the target stability (WMO, 2022). Both metrics are calculated at a global level using in situ observations as the reference, drifting buoys for the SST component and sea ice buoys and drifting stations for the IST component according to Ohring et al. (2005).

2. Validation results

This document applies to the L4 SST/IST CDR (1982-2021) and ICDR (2022-2023)[2] produced by C3S. These products are described in detail in the Product User Guide and Specification [D3] and Algorithm Theoretical Basis Document [D4]. For further details on the validation methodology see the Product Quality Assurance Document [D2].

2.1 SST Validation with In Situ data

Table 1 shows the median and robust standard deviation values along with the number of match-ups, between SST and in situ observations from drifting buoys, Argo floats, moored buoys and ships.

Table 1. Validation statistics comparing the L4 SST component to drifting buoys, tropical moored buoys, ARGO floats and ship-based measurements.

Type	Median	Robust Standard Deviation	Number of match-ups	Period
Drifting Buoys	-0.04	0.28	62684553	1982-2023
Argo floats	-0.04	0.23	1548956	2000-2023
Argo surface	-0.05	0.22	318034	2000-2023
Moored buoys	-0.04	0.17	248106	1998-2023
Ships	-0.12	0.89	32969998	1982-2023

2.1.1 Dependence on year

Figures 1 to 4 show the time-series of annual median difference, robust standard deviation and number of match-ups between the SST component of the SST/IST CDR/ICDR v1.0 and in situ observations from drifting and moored buoys, ships and Argo floats respectively.

The median difference between the SST component and drifting buoys (Figure 1) is consistently within the range -0.1 to 0.0 °C since around 1995 when the number of match-ups started to increase significantly while in the early period (1982-early 1990s) the median difference ranges mostly between -0.2 and 0.2 °C with very few match-ups. The robust standard deviation is in the range 0.4 to 0.25 °C from 1995 onwards while it remains rather constant at 0.25 °C from about mid 2000s and onwards.

[2]The ICDR for 2024 has not been included in the validation due to unavailability of the entire ICDR and corresponding in-situ observations for 2024 at the time of writing.

When moored buoys are used (Figure 2), the median difference stabilises around -0.1 °C from the mid-2000s and onwards while it varies between -0.2 and 0.2 °C between 1982 and 2004. The robust standard deviation decreases over the years from around 0.5 °C in the 1980s to 0.25 °C after 2000.

Ships pose a greater challenge (Figure 3) due to the depth difference between the in situ measurement and the 20 cm reference depth of the SST, which appears as higher values in the robust standard deviation although relatively stable throughout the record.

Argo and surface Argo floats (Figure 4a and b, respectively) show low and stable values for the median difference around 0.0 °C while the robust standard deviation is stable at 0.25 °C from 2004 (2012 for Argo surface) onward when the number of available observations increased.

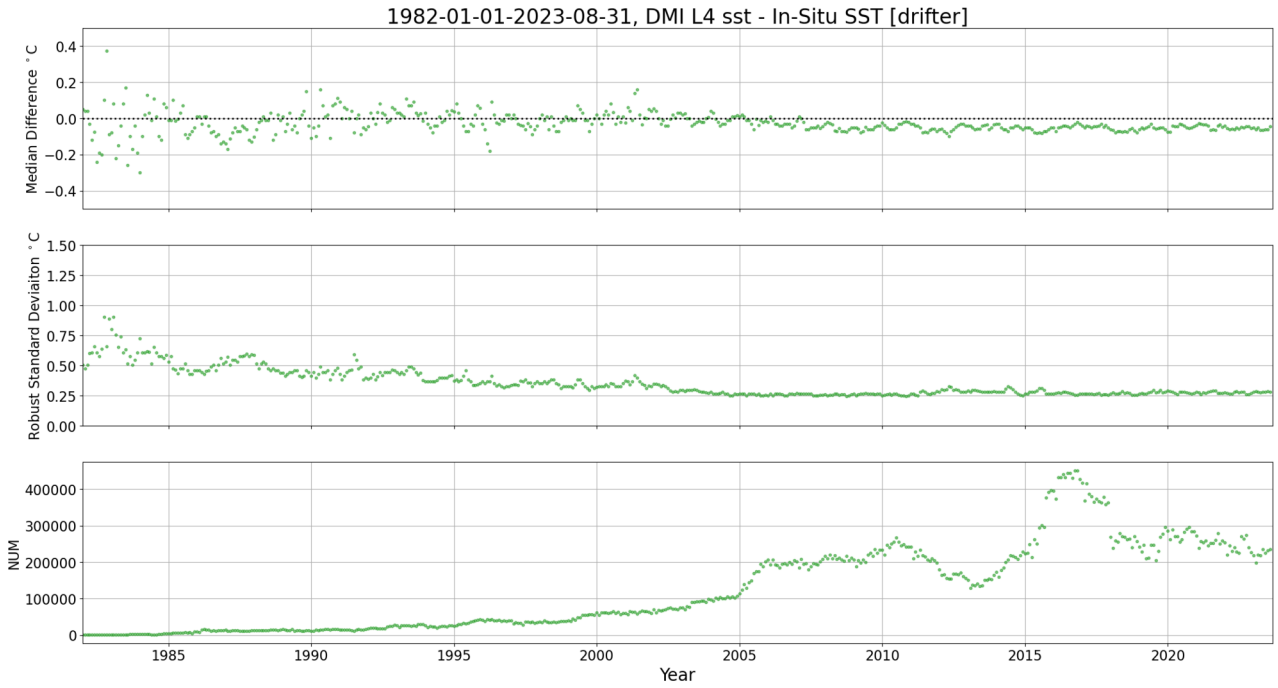

Figure 1. Time-series of SST median difference (top), robust standard deviation (middle) and number of match-ups (bottom) between the SST/IST CDR v1.0 and ICDR v1.0 and drifting buoys.

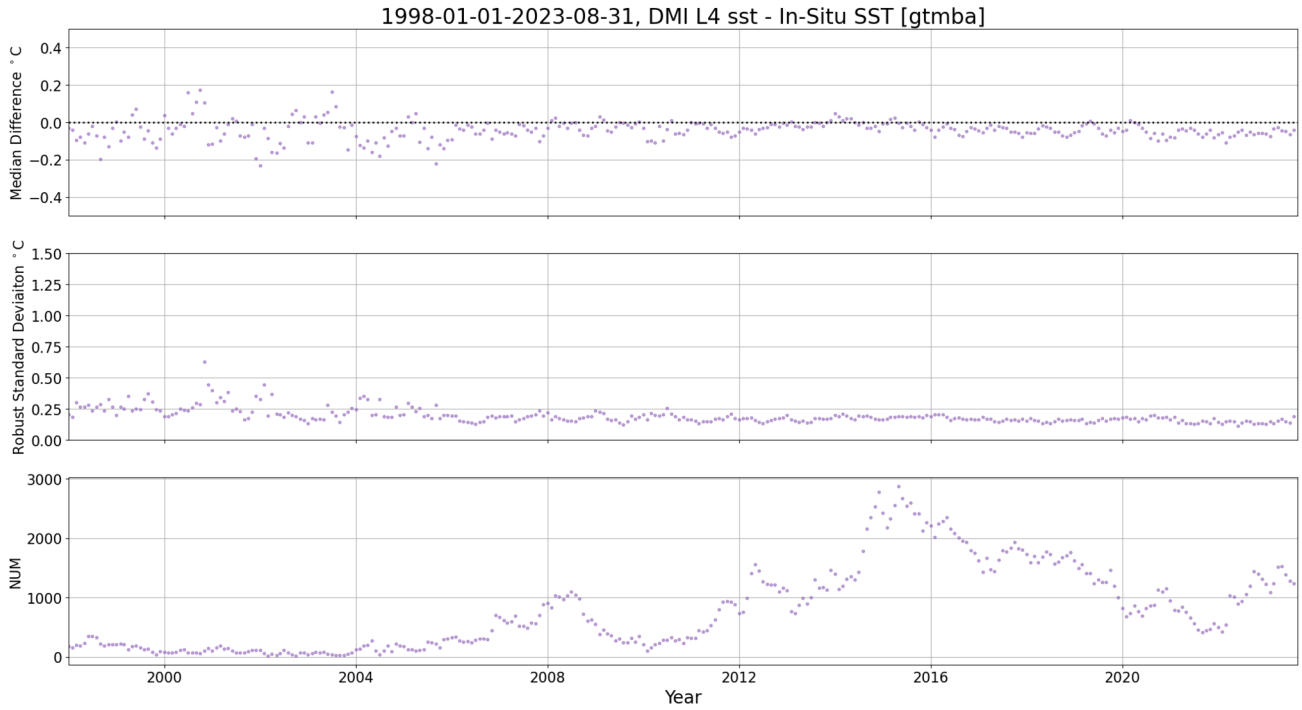

Figure 2. Time-series of SST median difference, robust standard deviation and number of match-ups between the SST/IST CDR v1.0 and ICDR v1.0 and moored buoys.

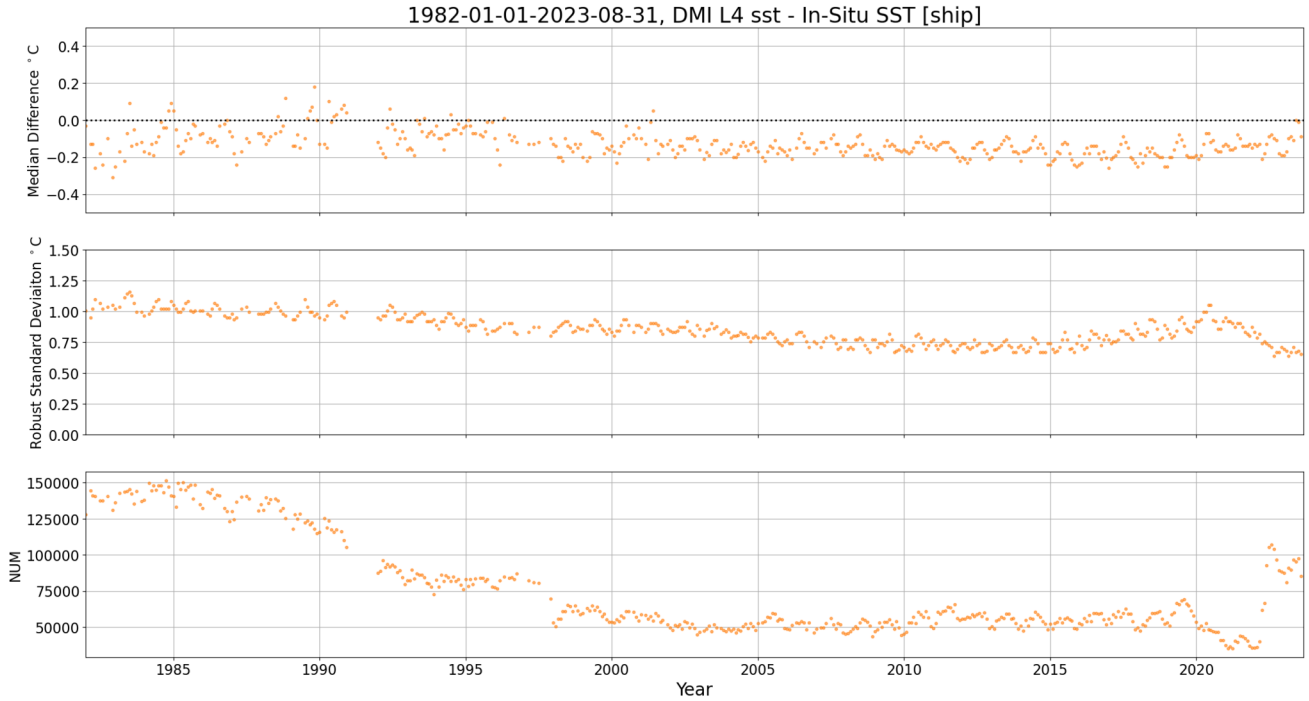

Figure 3. Time-series of SST median difference, robust standard deviation and number of match-ups between the SST/IST CDR v1.0 and ICDR v1.0 and ships.

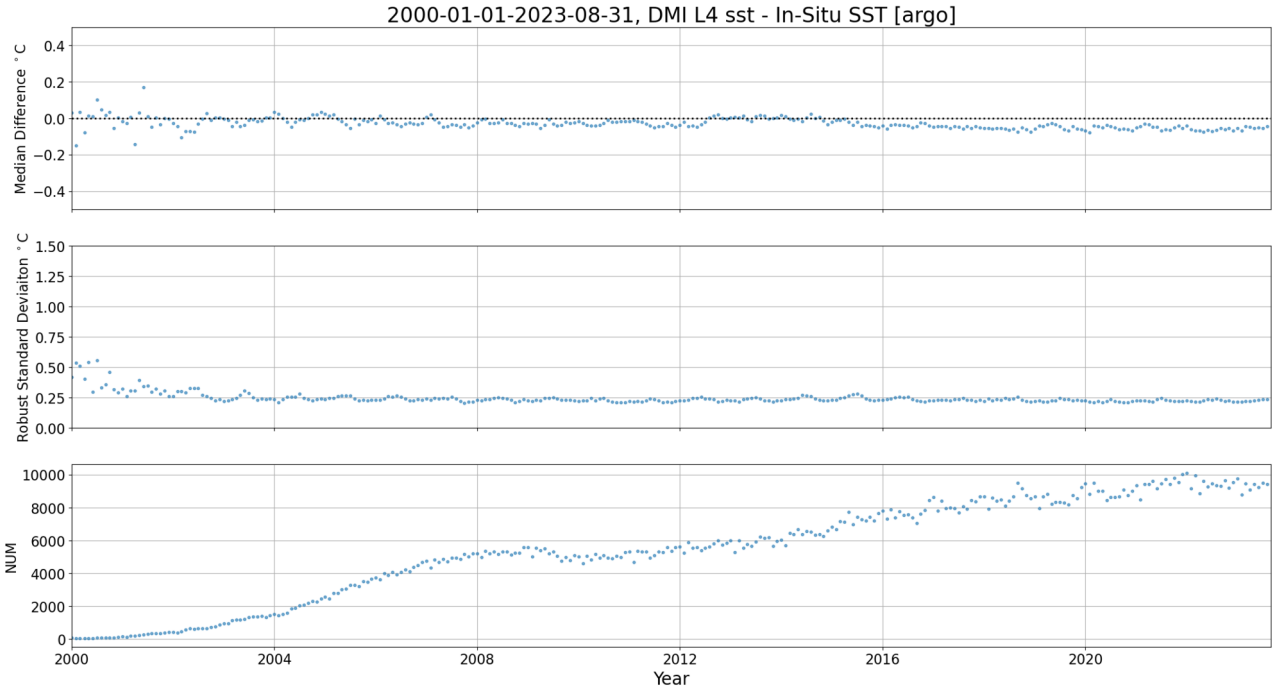

(a)

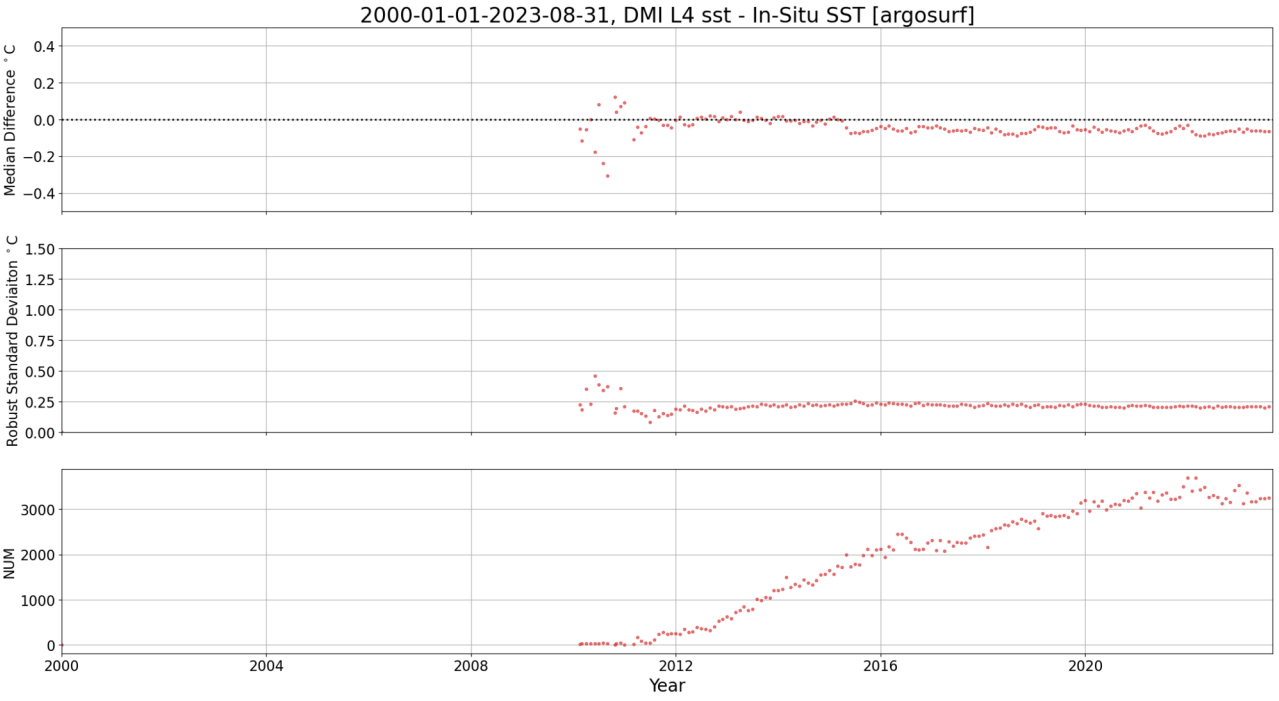

(b)

Figure 4. Time-series of SST median difference, robust standard deviation and number of match-ups between the SST/IST CDR v1.0 and ICDR v1.0 and (a) Argo and (b) surface Argo floats.

2.1.2 Dependence on latitude

Figures 5 to 8 show the latitude dependence of the (a) median difference, (b) robust standard deviation and (c) number of match-ups between the SST component of the SST/IST CDR/ICDR v1.0 and in situ observations from drifting and moored buoys, ships and Argo floats respectively.

When drifters are considered (Figure 5), the median difference is zero between 35°S and 35°N (Tropics and Sub-tropics), the robust standard deviation stable at 0.25 °C while the number of observations shows a decrease. Within the temperate zones, between 35° and 65° North and South, median differences turn slightly negative, between -0.1 and -0.2 °C, the robust standard deviation increases slightly and varies more – especially for the Northern Hemisphere – and the number of available observations increases.

This pattern is confirmed by the moored tropical buoys (Figure 6), limited between 20°S and 20°N. When ship observations are used (Figure 7), a higher median difference, from -0.1°C to -0.3°C, and robust standard deviation values (0.3°C to 1.0°C) are reported, more stable within the Tropics and Sub-tropics while the number of observations is highest within the temperate zone of the Northern Hemisphere.

For Argo and surface Argo (Figure 8a and 8b), median differences are almost zero between 40°S and 40°N, robust standard deviation is stable at 0.25°C and the number of observations highest for this region. A lower number of observations is recorded outside the 50°S and 50°N regions, although the median difference and robust standard deviation is lower for the Southern Hemisphere compared to the Northern one, typically associated with more dynamic oceanic features, e.g. the Gulf Stream.

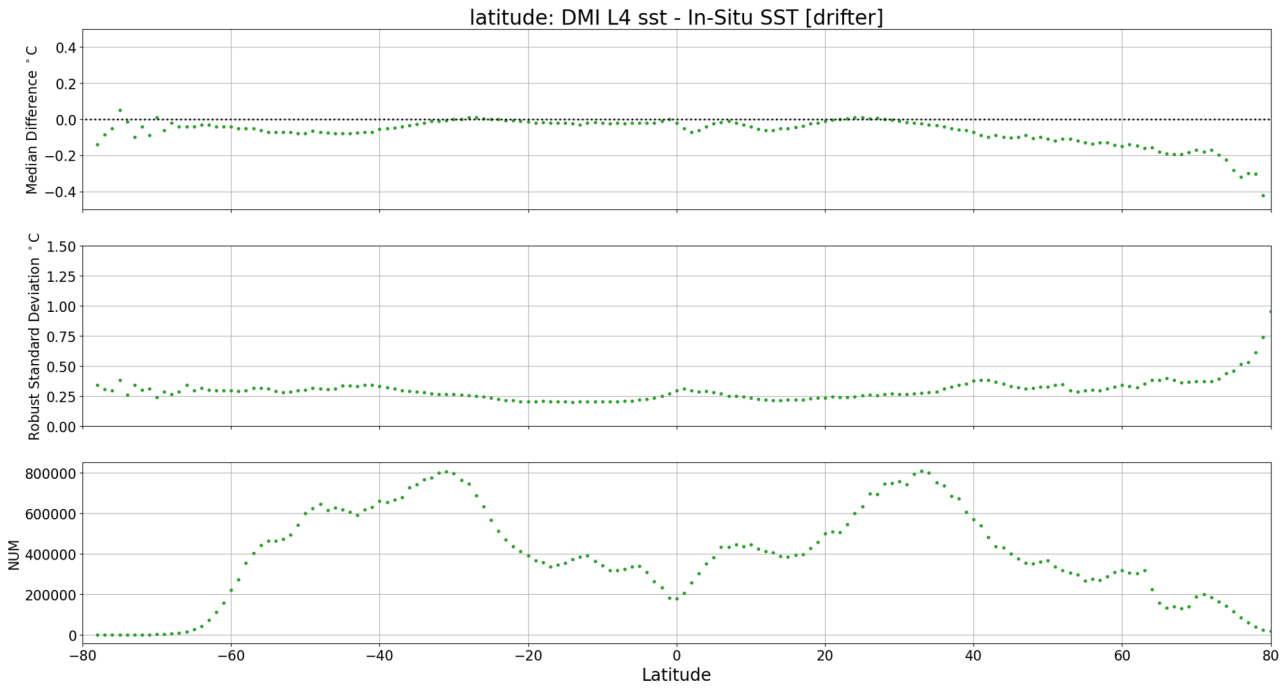

Figure 5. Latitude dependence of median difference (top), robust standard deviation (middle) and number of match-ups (bottom) between the SST component of the SST/IST CDR/ICDR v1.0 and drifting buoys.

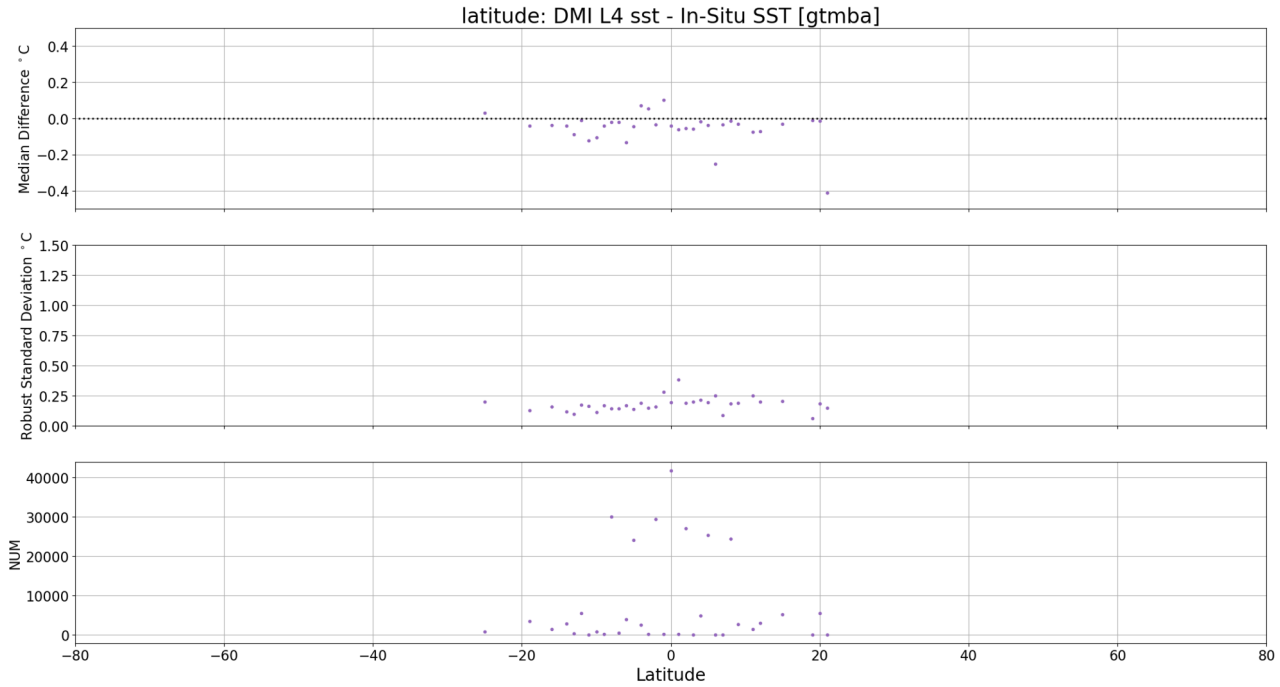

Figure 6. Latitude dependence of median difference top), robust standard deviation (middle) and number of match-ups (bottom) between the SST component of the SST/IST CDR/ICDR v1.0 and moored buoys.

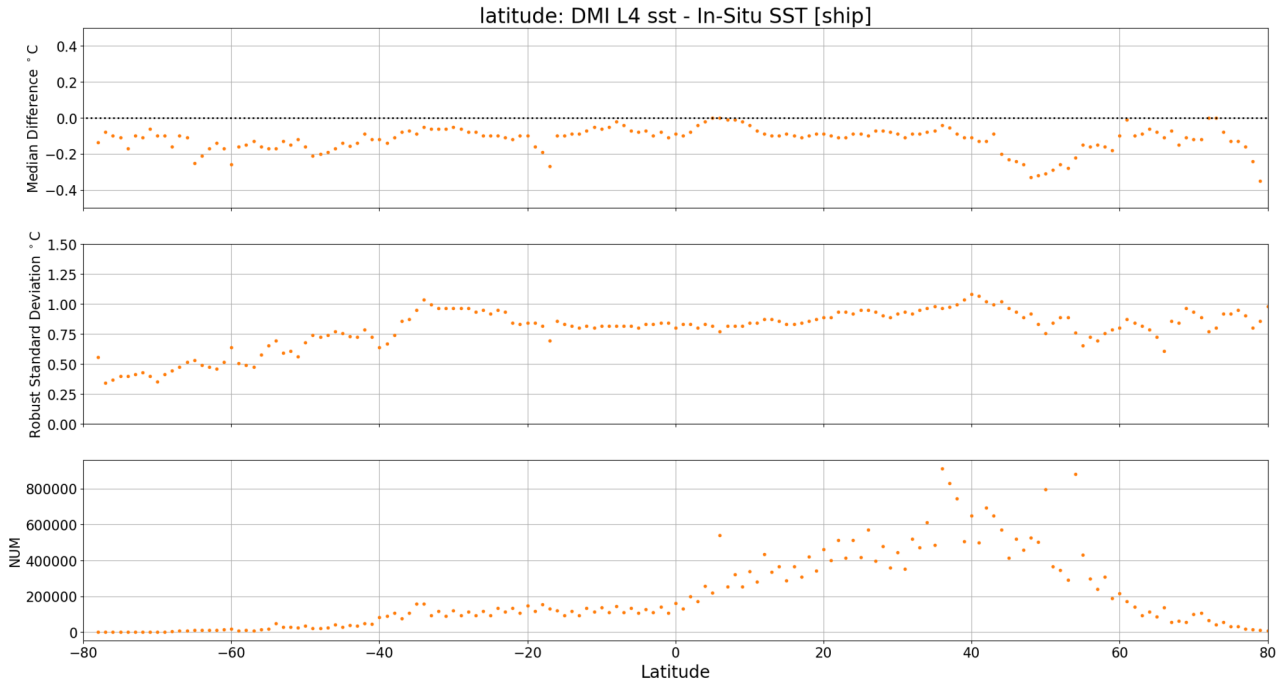

Figure 7. Latitude dependence of median difference top), robust standard deviation (middle) and number of match-ups (bottom) between the SST component of the SST/IST CDR/ICDR v1.0 and ships.

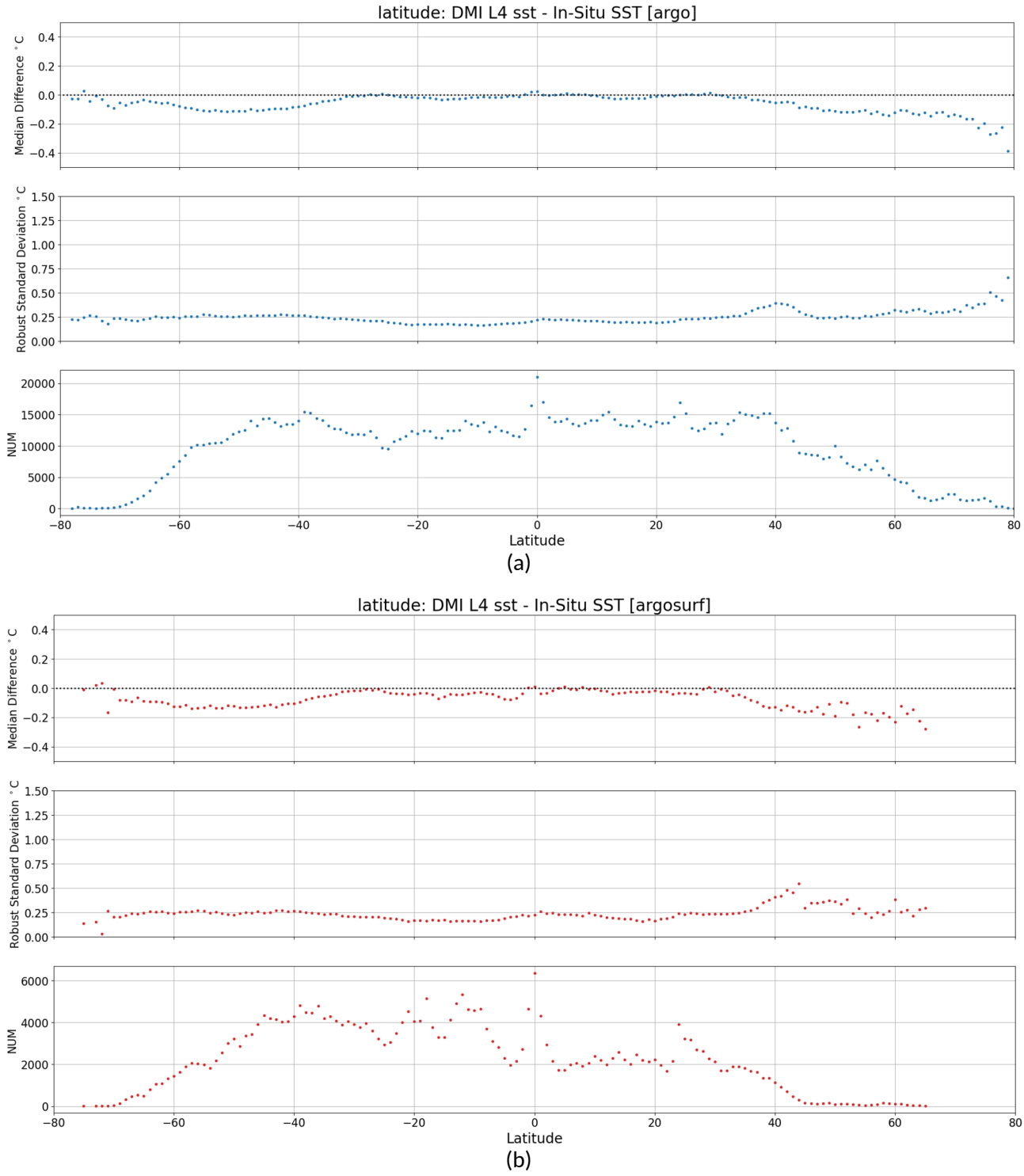

Figure 8. Latitude dependence of median difference (top), robust standard deviation (middle) and number of match-ups (bottom) between the SST component of the SST/IST CDR/ICDR v1.0 and Argo floats (a: all, b: surface only).

2.1.3 Spatial distribution

Figures 9 to 13 show the spatial distribution dependence of the (a) median difference, (b) robust standard deviation and (c) number of match-ups between the SST component of the SST/IST CDR/ICDR v1.0 and in situ observations from drifting and moored buoys, ships and Argo floats respectively.

For drifting buoys (Figure 9), median differences of around zero are identified in large parts of the global ocean tending to be slightly positive (indicating warmer L4 SST compared to in situ) in the Indian Ocean, Mediterranean, Baltic and Red Seas and around Indonesia and the Philippines. Slightly negative median differences are found in the western boundaries of Africa, North and South America and at high latitudes close to the Arctic ocean and Antarctica. The robust standard deviation is less than 0.2°C for the largest parts of the global ocean while it increases up to 1°C in dynamic regions of major current systems. The number of observations is significantly higher in the North Atlantic and parts of the South Atlantic compared to other regions of the global ocean.

For the moored buoy observations (Figure 10), median differences are variable, mostly close to zero for the Tropical Atlantic, slightly positive (indicating higher C3S L4 SST/IST values) for the Indian Ocean and slightly negative for the Tropical Pacific, although always ranging between -0.1°C and 0.1°C. The robust standard deviation is within 0.2°C for all tropical regions and the number of observations is relatively stable, between 500 and 1500 match-ups, for most of the moorings with the exception of some moorings in the Tropical Pacific where match-ups range between 2500 and 4000.

When ships are considered (Figure 11), median differences are highly variable and mostly range between -0.4°C and 0.4°C, the robust standard deviation is higher in the Northern Hemisphere compared to the Southern Hemisphere and the central Pacific Ocean, and it is especially high in very dynamic regions of major current systems where the number of observations is also highest.

For the Argo and Argo surface observations (Figure 12 and Figure 13 respectively), similar findings to those for the drifting buoys are reported, with median differences around zero identified in large parts of the global ocean tending to be slightly positive (indicating warmer L4 SST compared to in situ) in the Indian Ocean, Mediterranean Sea, Sub-tropical Atlantic and Pacific Ocean and around Indonesia and the Philippines. Slightly negative median differences are found in the western boundaries of Africa, North and South America and at high latitudes close to the Arctic ocean and Antarctica. The robust standard deviation is less than 0.2°C for the largest parts of the global ocean while it increases up to 1°C in dynamic regions of major current systems. The number of observations is significantly higher in the Northern Hemisphere compared to the Southern one, with observations mostly found in the Gulf of Mexico, Sea of Japan and East China Sea, Mediterranean, Arabian and Labrador Seas, Bay of Bengal and the southern part of the Gulf of Alaska.

(a)

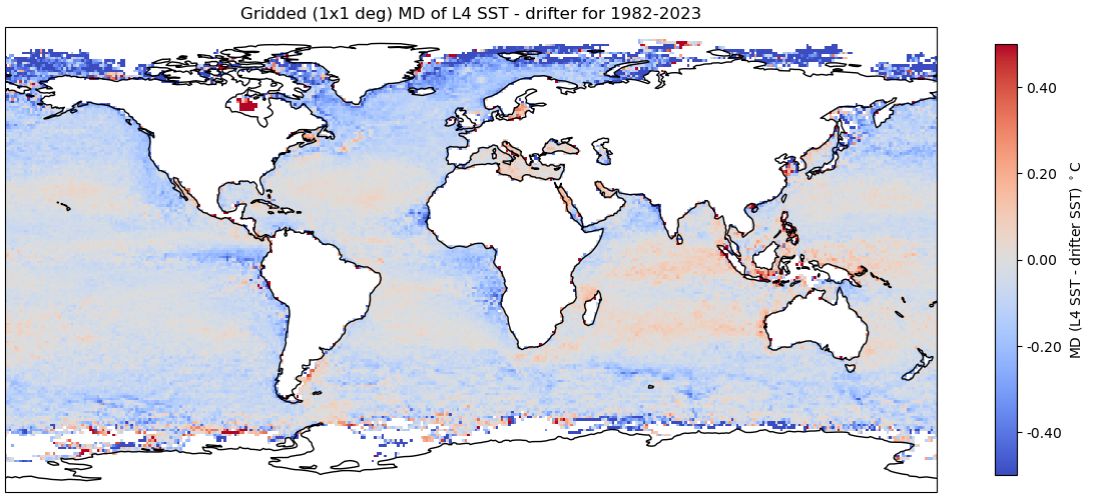

(b)

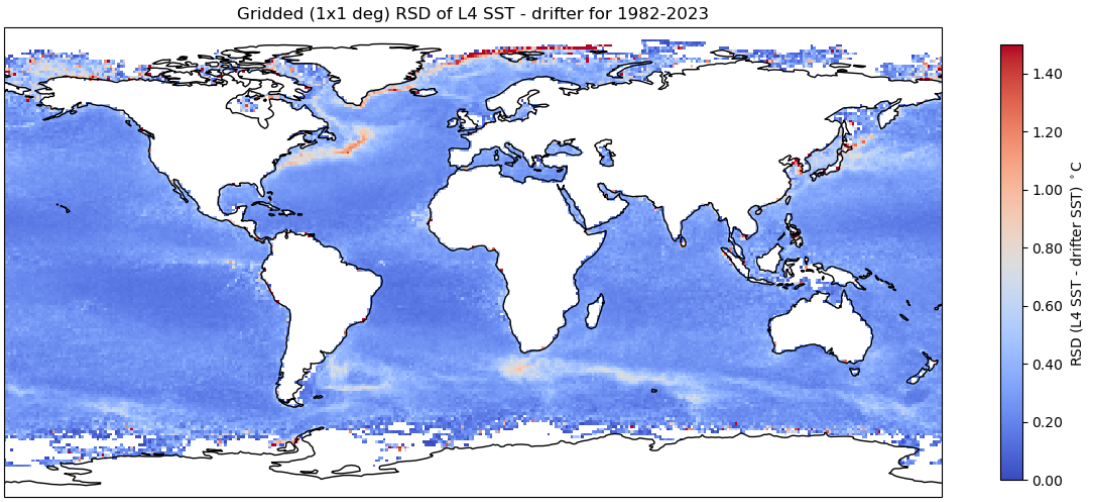

(c)

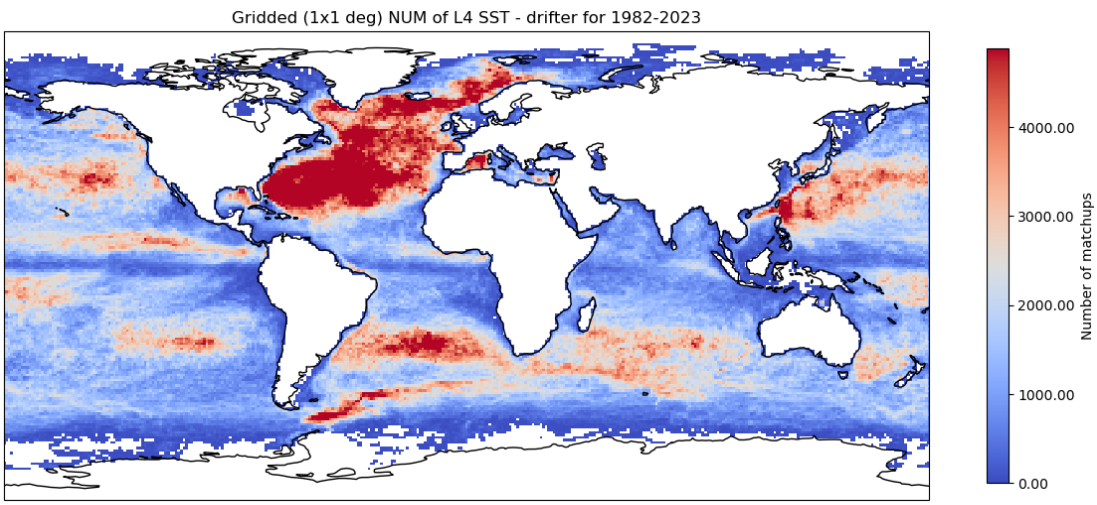

Figure 9. Spatial distribution of median difference (a), robust standard deviation (b) and number of match-ups (c) between the SST component of the SST/IST CDR/ICDR v1.0 and drifting buoys.

(a)

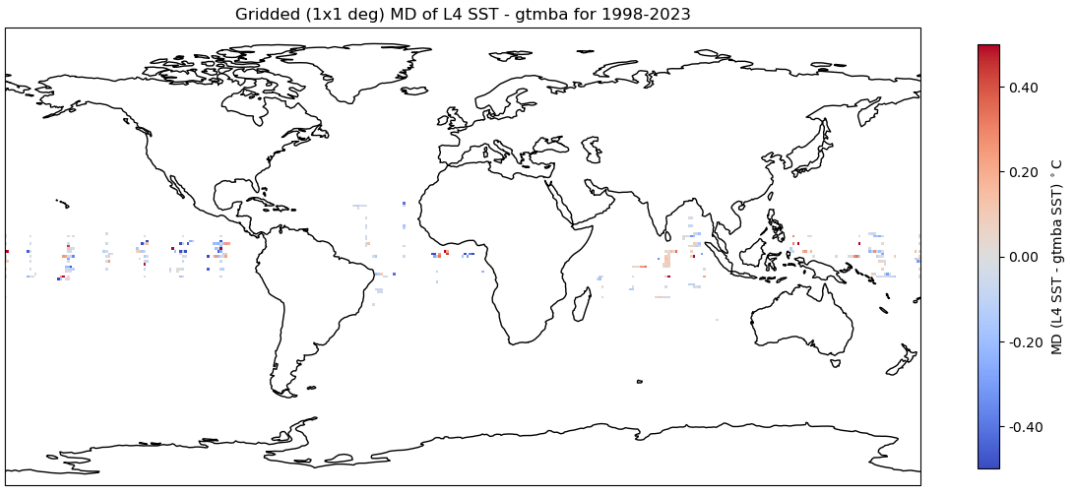

(b)

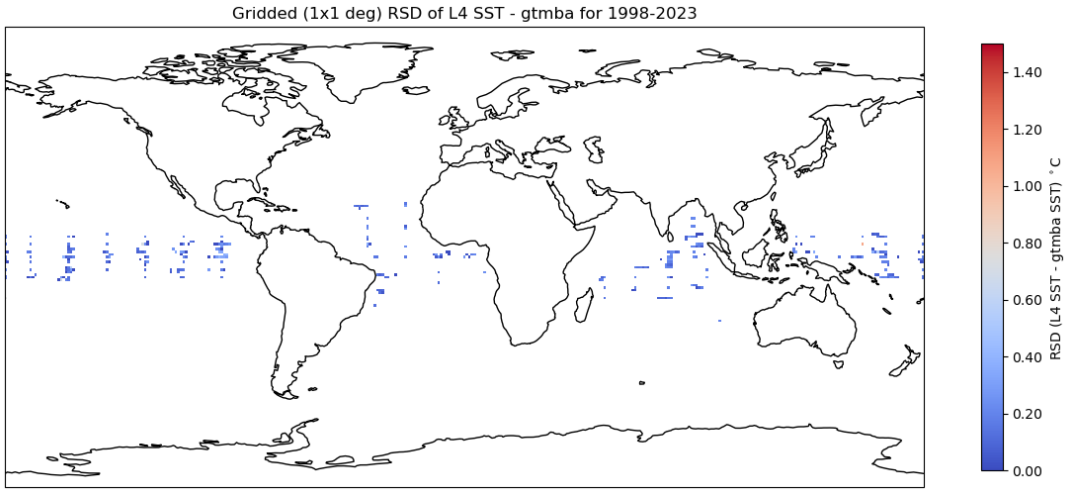

(c)

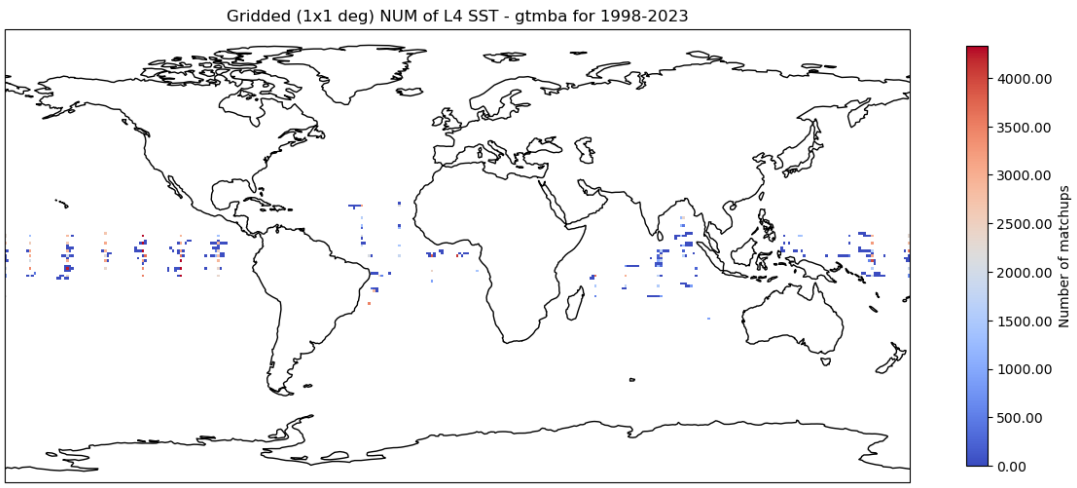

Figure 10. Spatial distribution of median difference (a), robust standard deviation (b) and number of match-ups (c) between the SST component of the SST/IST CDR/ICDR v1.0 and moored buoys from the Global Tropical Moored Buoy Array (gtmba).

(a)

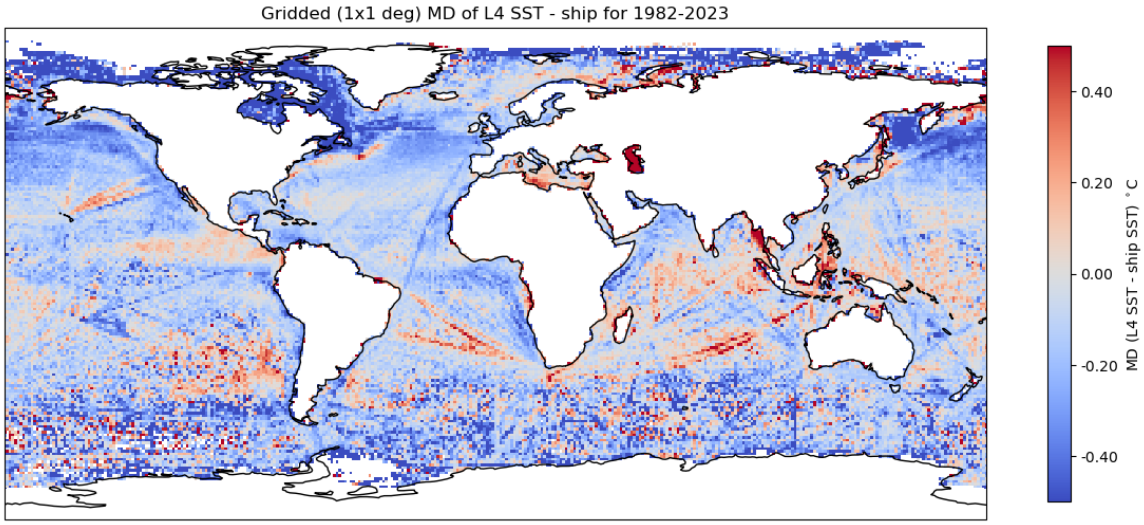

(b)

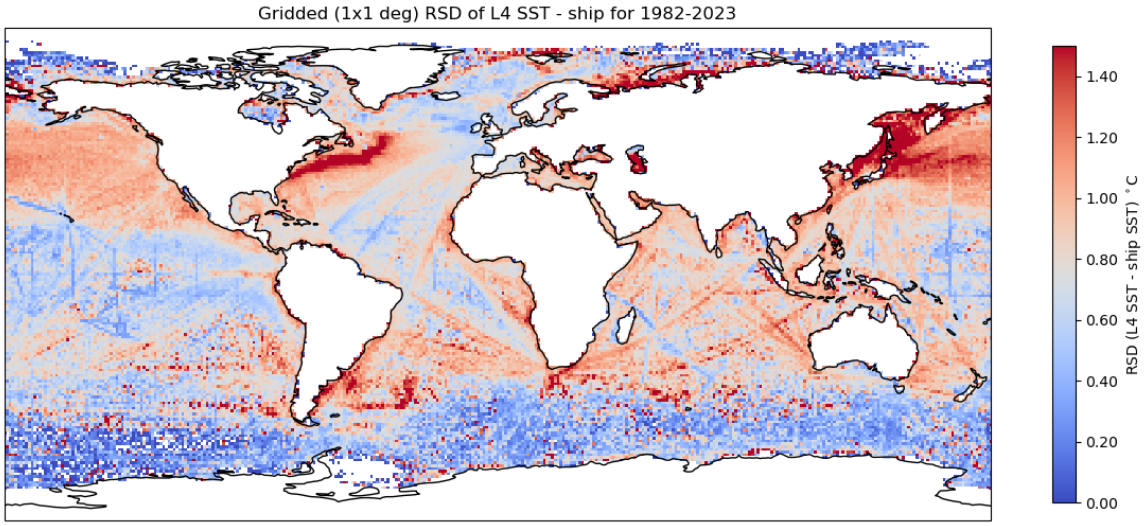

(c)

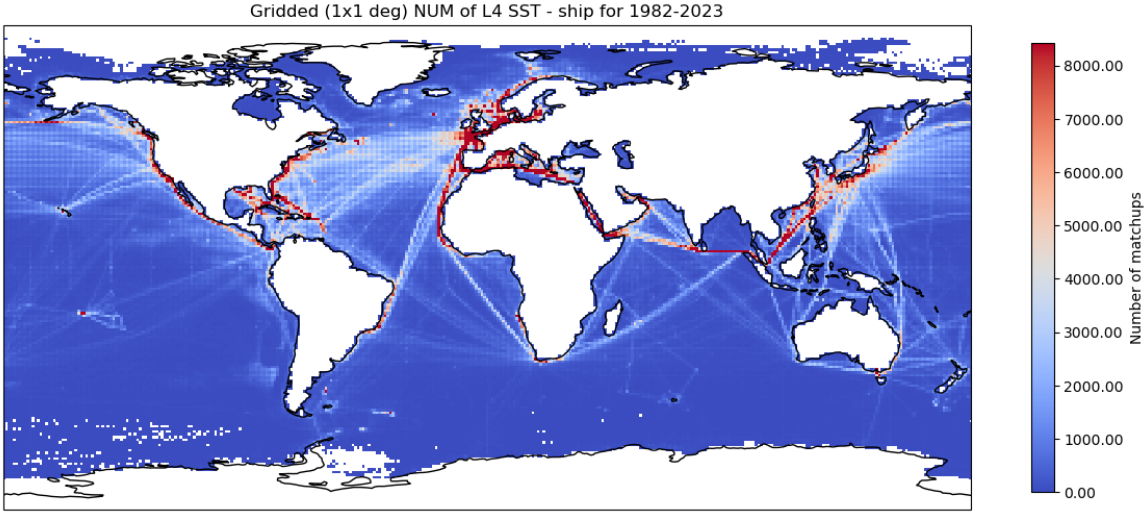

Figure 11. Spatial distribution of median difference (a), robust standard deviation (b) and number of match-ups (c) between the SST component of the SST/IST CDR/ICDR v1.0 and ships.

(a)

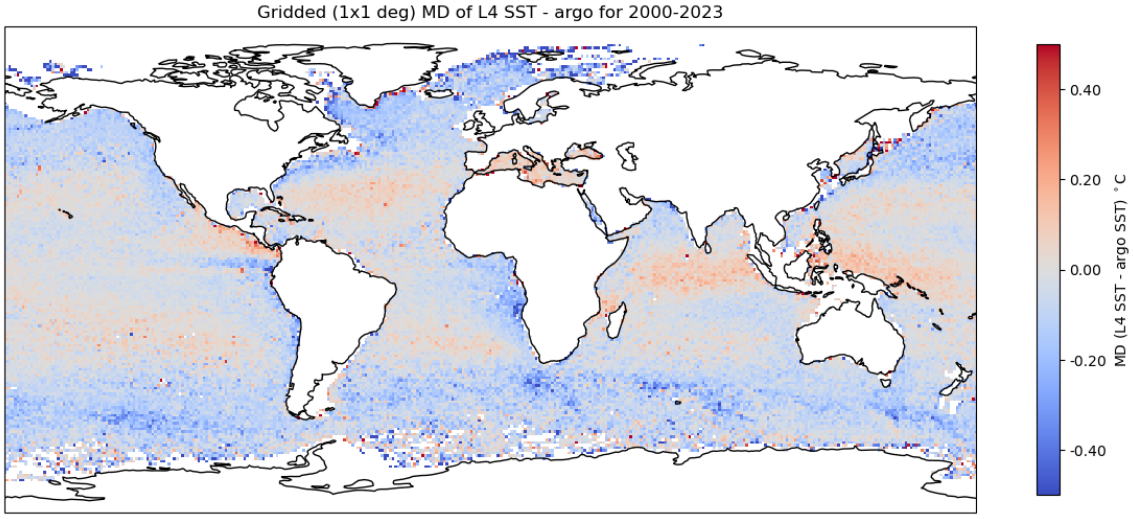

(b)

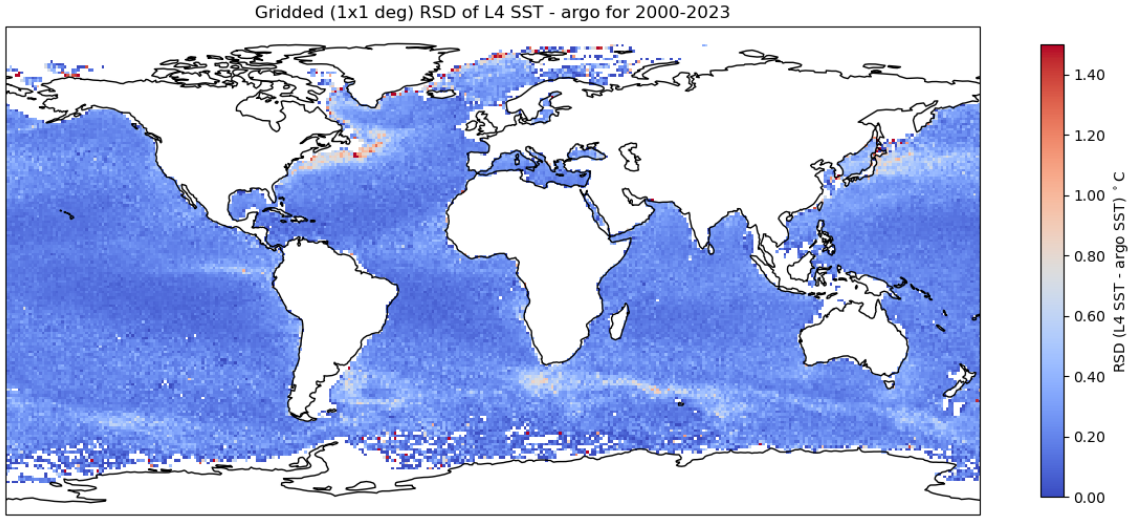

(c)

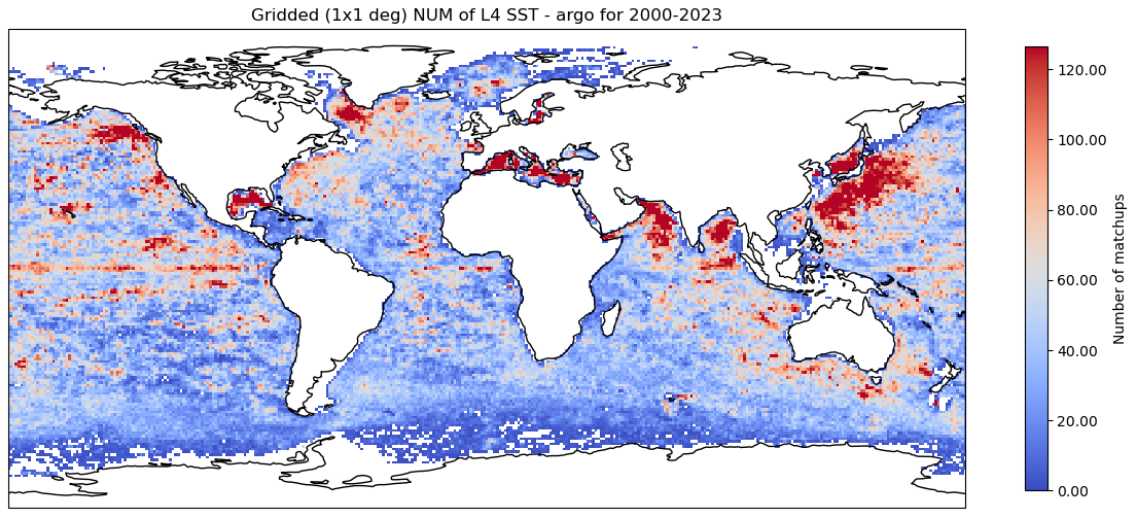

Figure 12. Spatial distribution of median difference (a), robust standard deviation (b) and number of match-ups (c) between the SST component of the SST/IST CDR/ICDR v1.0 and Argo.

(a)

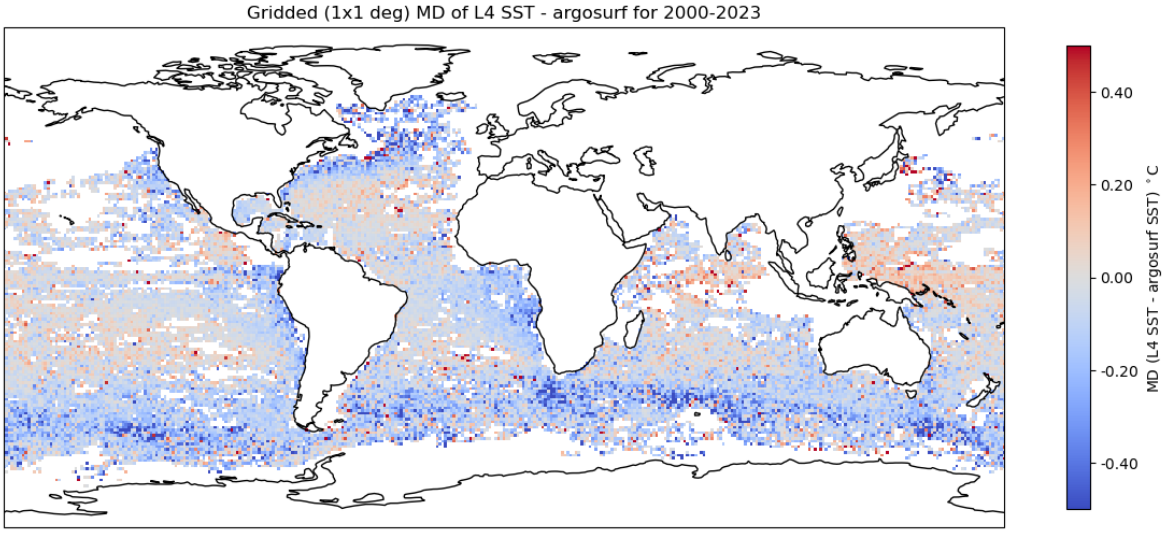

(b)

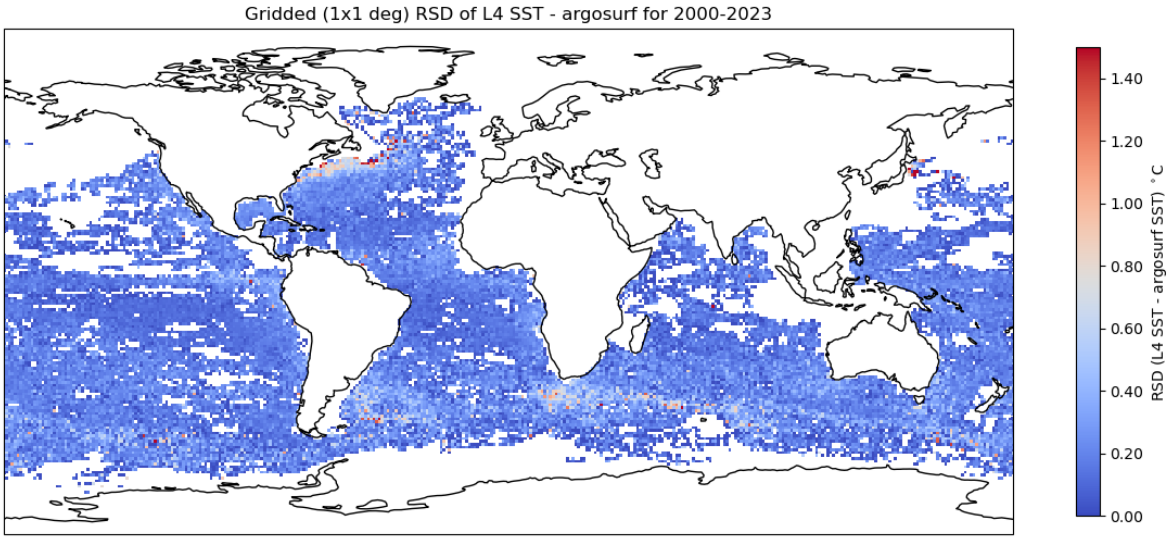

(c)

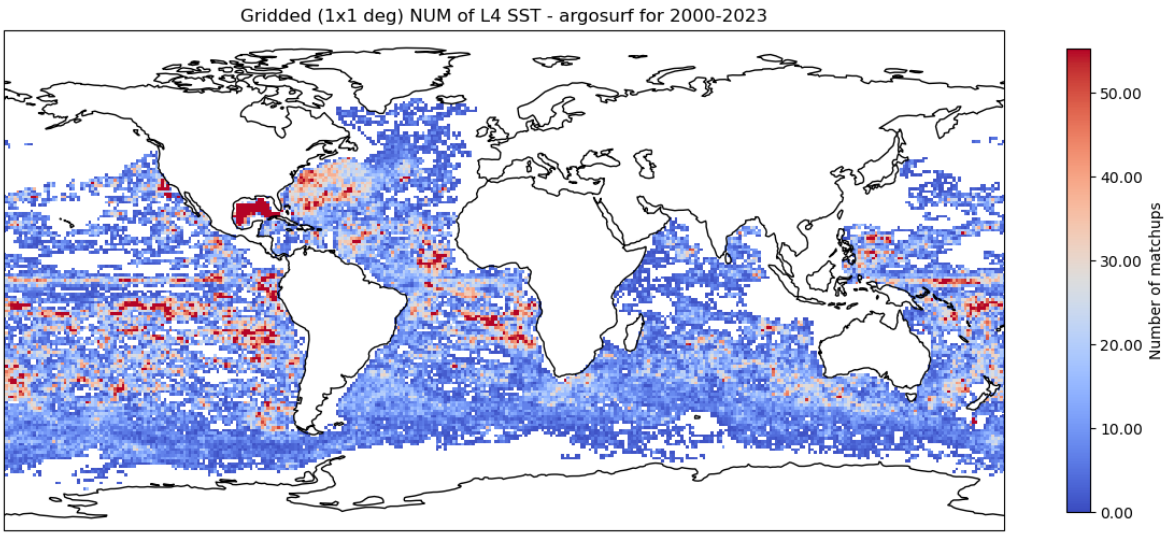

Figure 13. Spatial distribution of median difference (a), robust standard deviation (b) and number of match-ups (c) between the SST component of the SST/IST CDR/ICDR v1.0 and Argo surface.

2.1.4 Hovmöller distribution

Hovmöller diagrams (or distributions) depicting the gridded median bias between the SST component of the C3S Global L4 SST/IST product and in situ observations from drifters in Figure 14, (a) moored buoys and (b) ships in Figure 15, while Argo (a) and surface Argo floats (b) are presented in Figure 16, as a function of time (horizontal axes) and latitude (vertical axes). For drifters (Figure 14), higher absolute median biases are confined to the earlier years (up to 1993) for both hemispheres and the Arctic region for the later years, with biases moderating at temperate and equatorial latitudes, and the Antarctic region as time goes on. For the tropical moored buoys array (Figure 15a), no significant change in the median bias with the year is observed although more moorings are available from 2007 onward. For ships (Figure 15b) higher negative median biases are reported for the high latitudes of both hemispheres throughout the record of data availability while zero and slightly positive median biases are reported for the mid-latitudes and the Tropics. Argo and surface Argo (Figure 16a and b respectively) floats show zero and slightly positive median differences for the Tropics and mid-latitudes throughout the record, which starts at approximately the year 2000. More negative median differences are confined to the higher latitudes and especially for the Arctic after 2018, similar to what was reported for the drifting buoys.

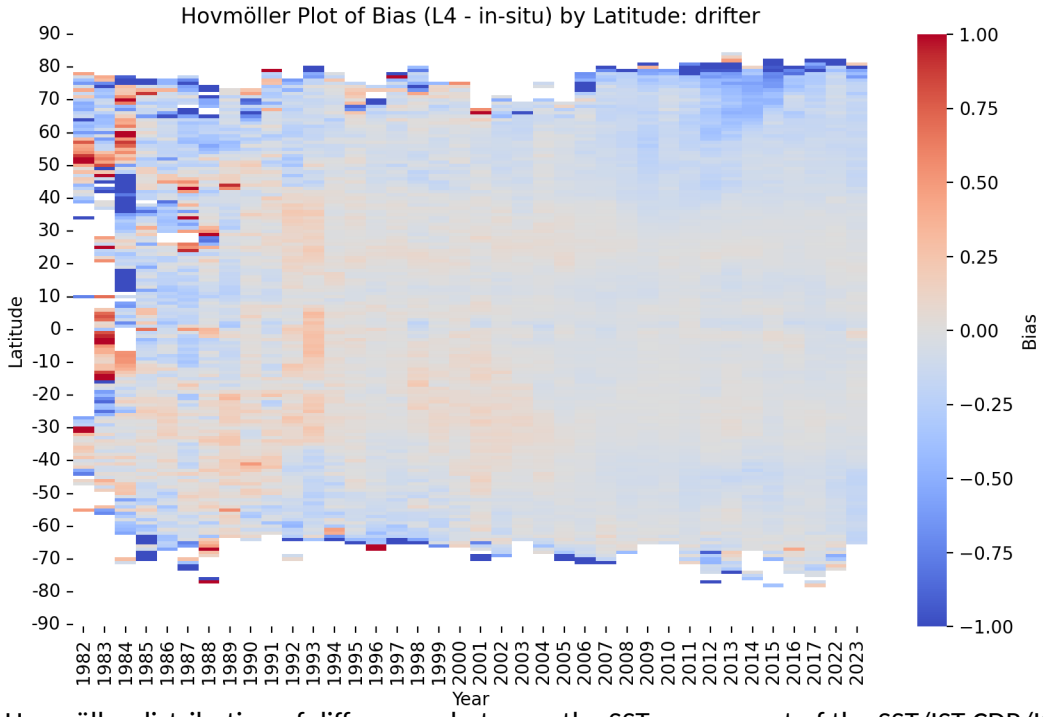

Figure 14. Hovmöller distribution of differences between the SST component of the SST/IST CDR/ICDR v1.0 and drifting buoys.

(a)

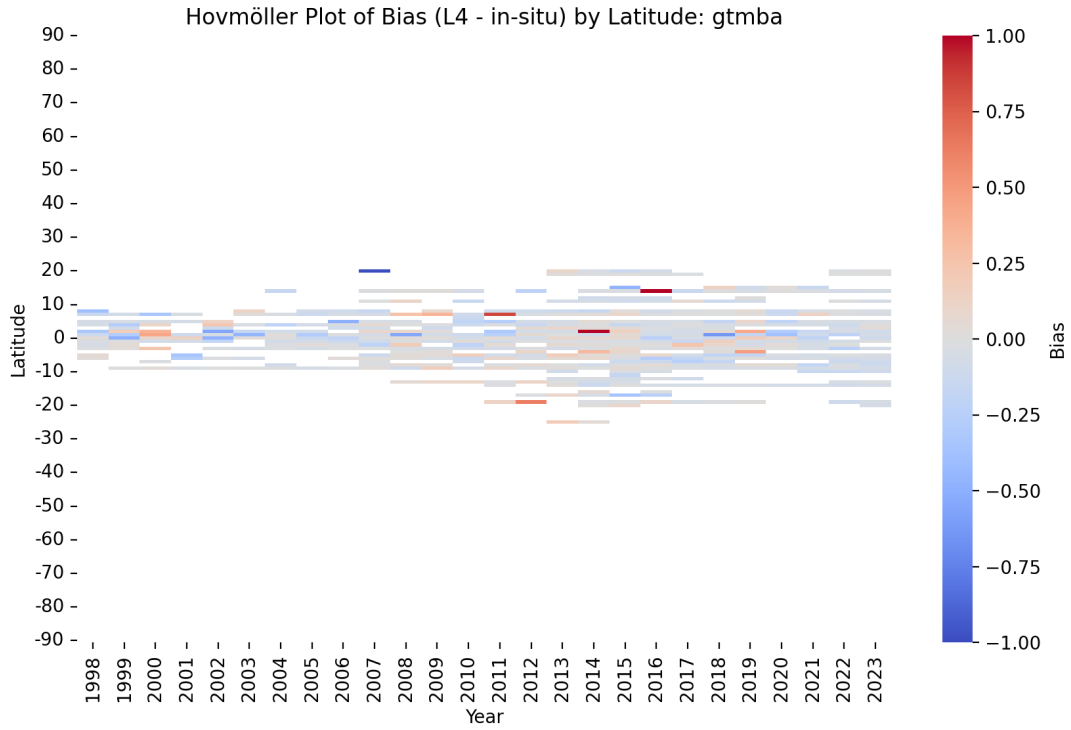

(b)

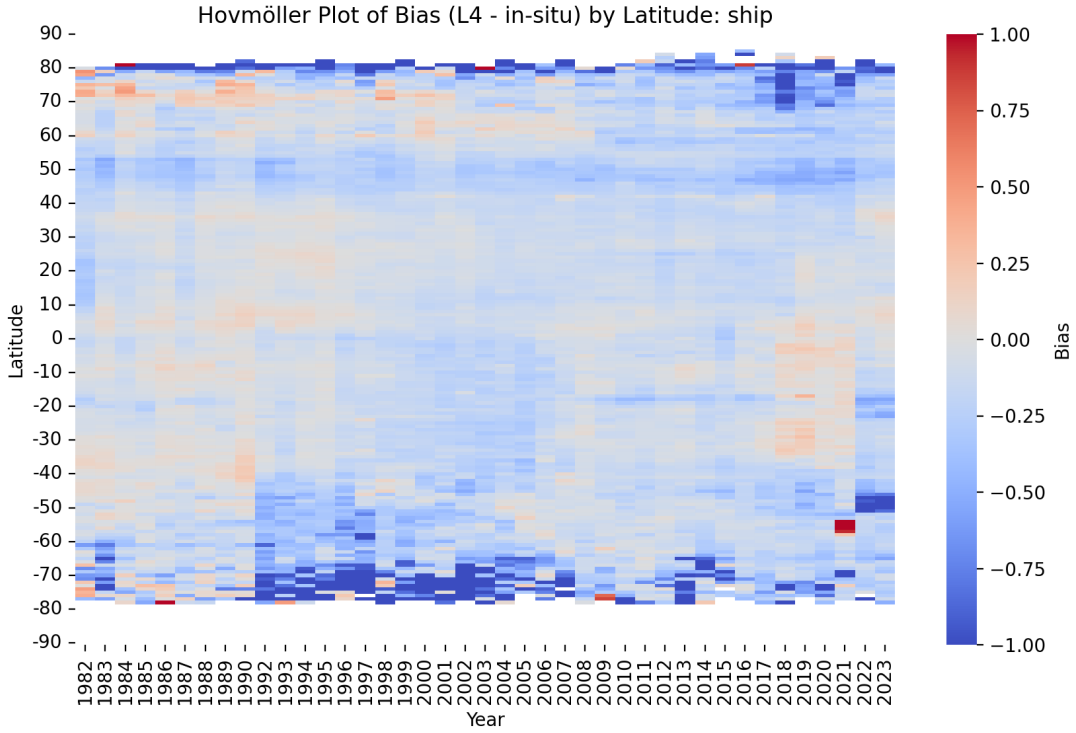

Figure 15. Hovmöller distribution of differences between the SST component of the SST/IST CDR/ICDR v1.0 and a) moored buoys, and b) ships.

(a)

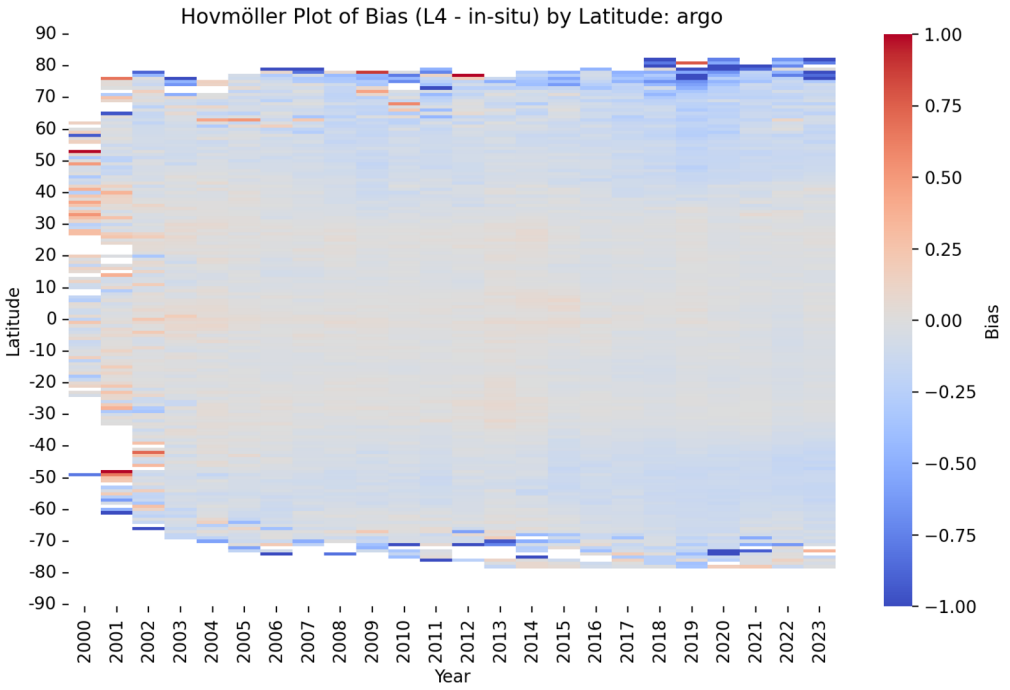

(b)

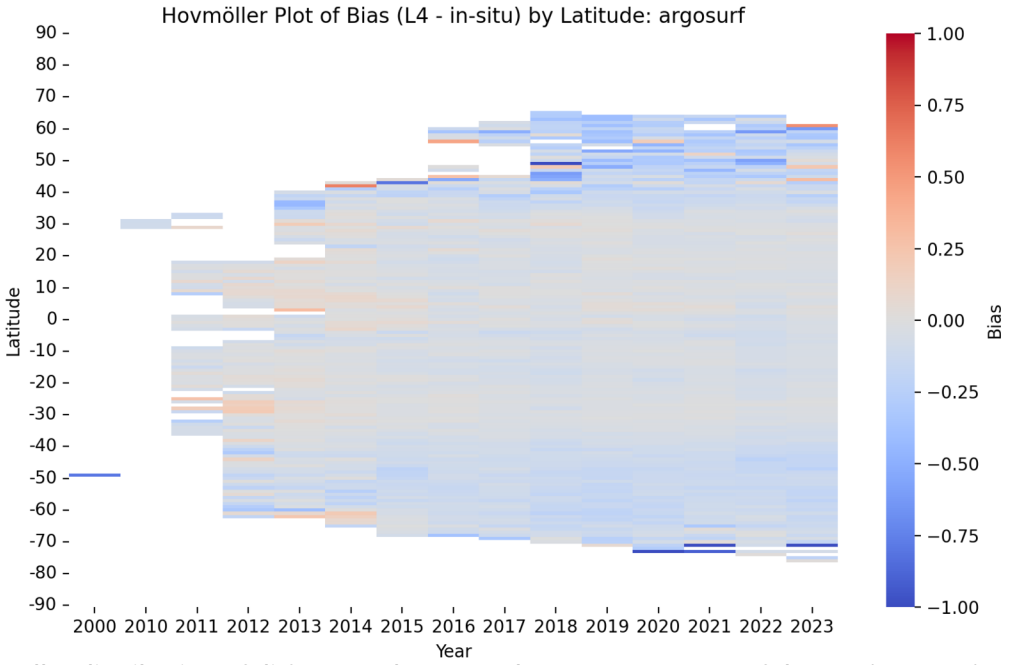

Figure 16. Hovmöller distribution of differences between the SST component of the SST/IST CDR/ICDR v1.0 and (a) Argo floats, and (b) surface Argo floats.

2.1.5 Histogram distribution

The histograms of frequency occurrence (vertical axes) of the median bias (horizontal axes) between the SST component of the C3S Global L4 SST/IST product and in situ observations from drifters are shown in Figure 17. Moored buoys (a) and ships (b) are shown in Figure 18 while Figure 19 shows the histograms for Argo (a) and (b) surface Argo floats. Especially for the drifters (Figure 17), moored buoys (Figure 18a), Argo and surface Argo floats (Figure 19 (a) and b), the histograms are well centred around zero while almost zero occurrences of median biases higher than 1°C to 1.5°C are identified. For ships (Figure 18 b), the histogram is slightly skewed towards negative values indicating higher ship temperatures, while the tails exceed 3 °C, consistent with what is known about the quality and relevance, or applicability, of ship measurements for validating SST_{20cm} especially since the placement of the ship-borne sensor is at depths well below the 20 cm reference depth. For Argo (Figure 19a) and surface Argo floats (Figure 19b), histograms are similar to the one for drifting buoys, although the peak is skewed to slightly negative values while almost zero occurrences of median biases higher than 1°C to 1.5°C are identified.

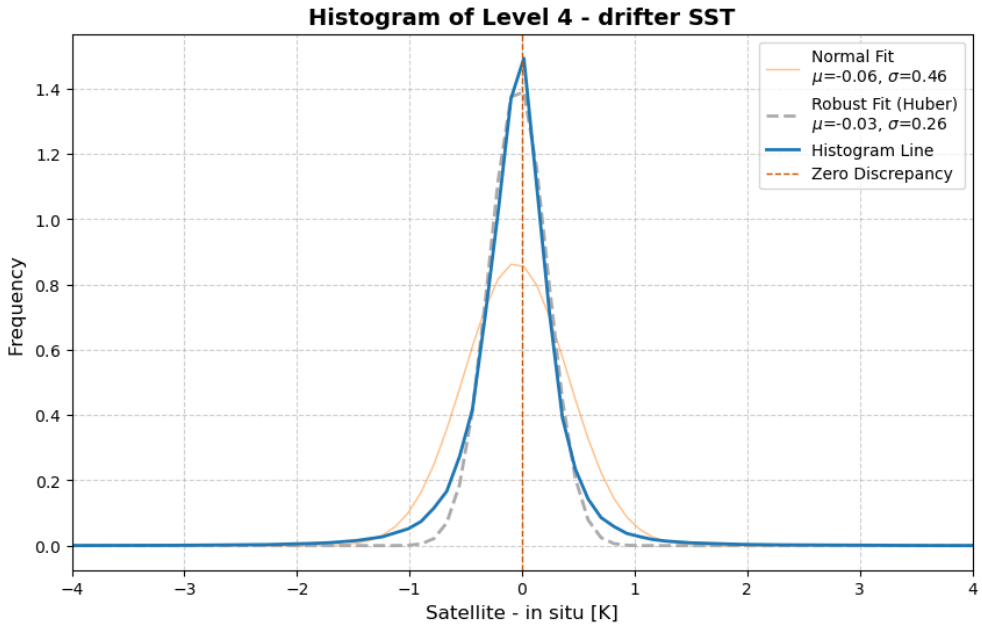

Figure 17. Histogram distribution of differences between L4 SST the SST component of the SST/IST CDR/ICDR v1.0 and drifting buoys.

(a)

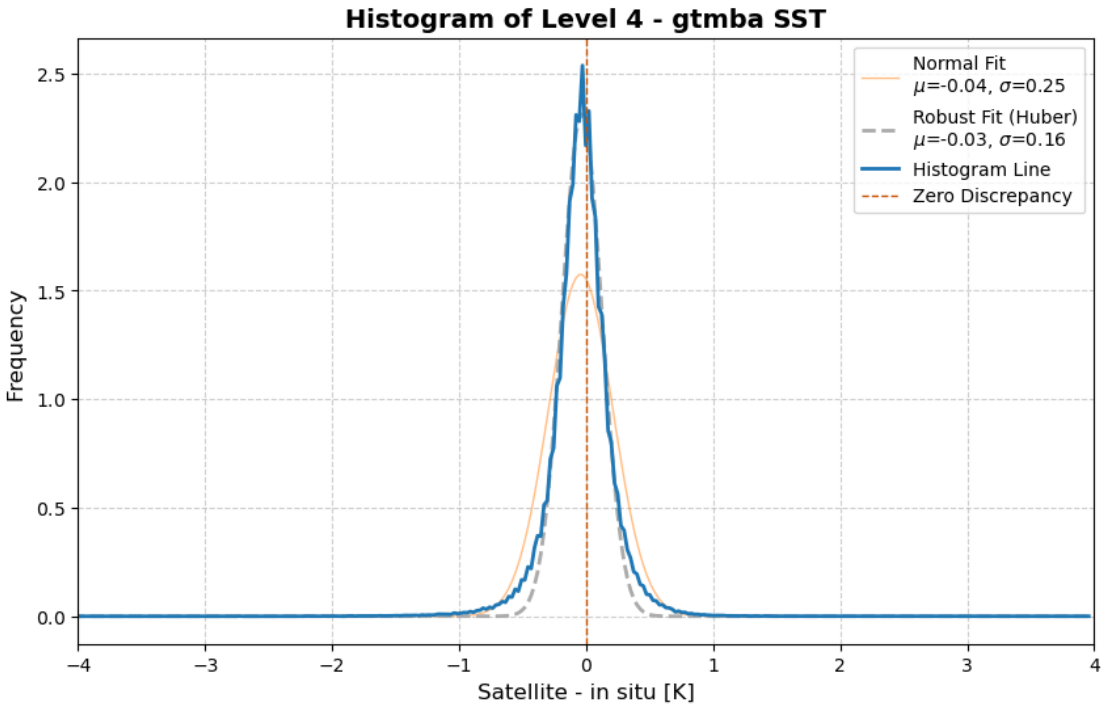

(b)

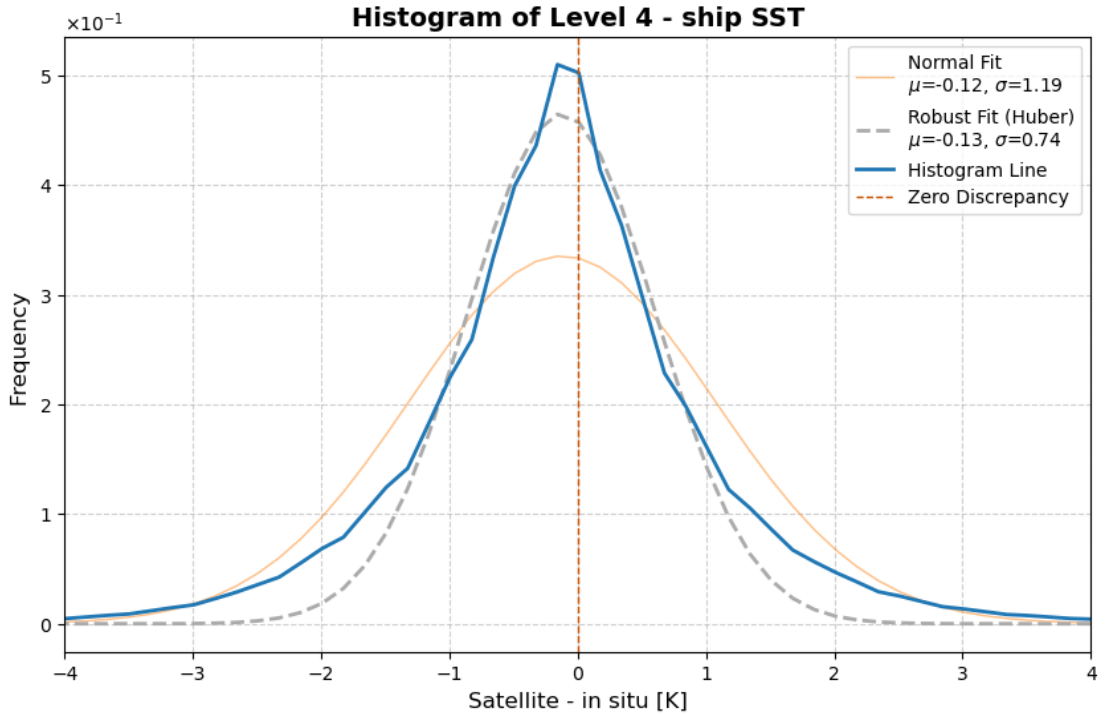

Figure 18. Histogram distribution of differences between L4 SST the SST component of the SST/IST CDR/ICDR v1.0 and a) moored buoys, and b) ships

(a)

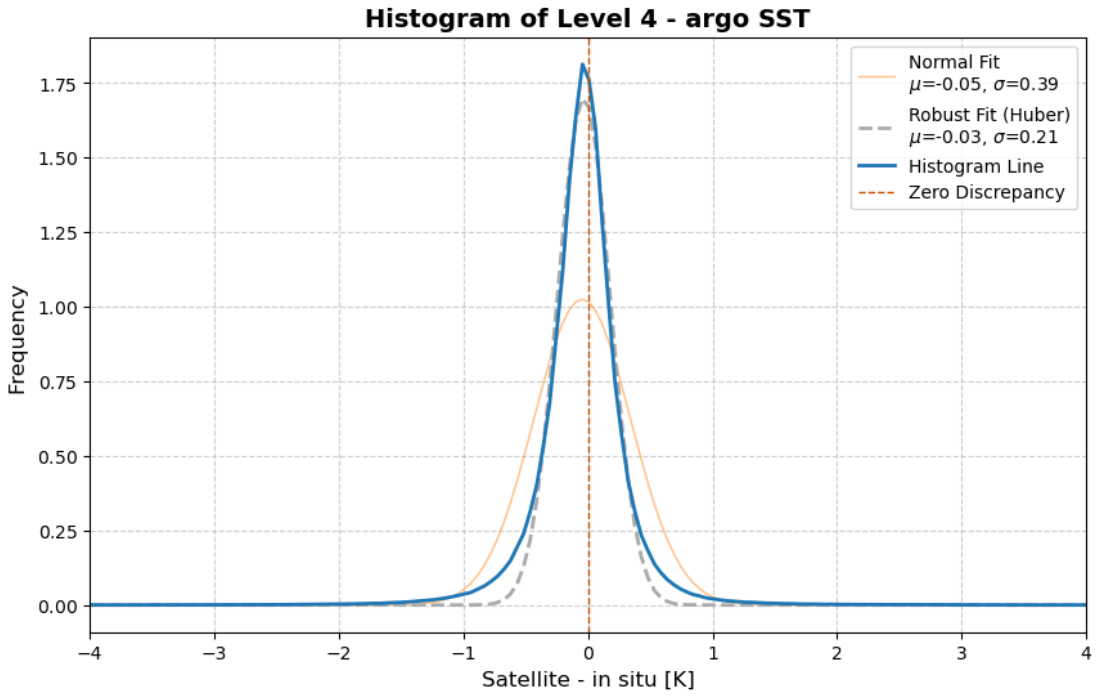

(b)

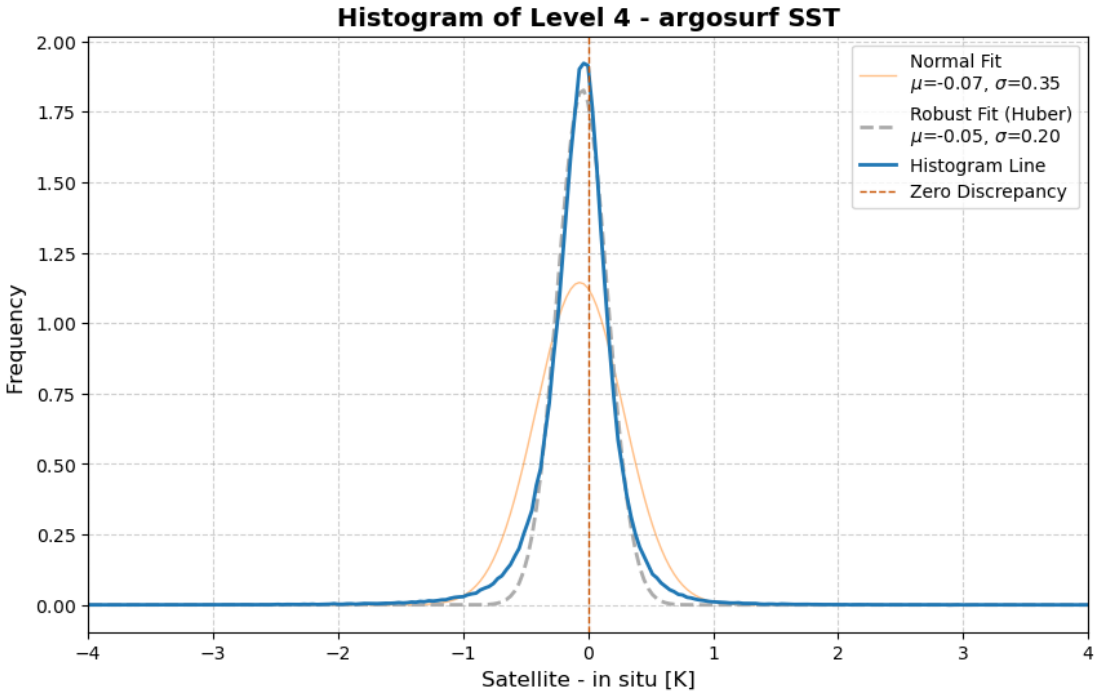

Figure 19. Histogram distribution of differences between L4 SST the SST component of the SST/IST CDR/ICDR v1.0 anda) Argo floats and b) surface Argo floats.

2.2 IST Validation with In Situ data

Table 2 shows the median and robust standard deviation values along with the number of match-ups computed between IST and in situ air temperature measurements from different types of buoys and skin surface temperatures from the IceBridge flights.

Table 2. Validation statistics comparing the L4 IST component to 2-m air temperature measurements (ECMWF, CRREL, SIMB3 and NP drifting ice stations) and skin surface temperature measurements (IceBridge flights), in both the Northern Hemisphere (NH) and Southern Hemisphere (SH).

Type	Median (°C)	Robust Standard Deviation (°C)	Number of match-ups	Period
ECMWF buoys NH (SH)	-3.13 (-3.24)	3.38 (3.09)	57611 (1912)	1993-2015 (1999-2009)
CRREL buoys NH	-2.73	3.44	23764	2001-2017
NP drifting ice stations	-2.24	3.36	8106	1983-1991 & 2003-2012
SIMB3 (NH)	-2.54	3.24	5831	2019-2023
IceBridge flights NH (SH)	1.39 (-2.72)	2.52 (1.85)	40884 (611)	2012-2019 (2013)

2.2.1 Dependence on year

Figures 16 to 20 show the time-series of annual median difference, robust standard deviation and number of match-ups between the IST component of the SST/IST CDR/ICDR v1.0 and in situ observations from the ECMWF, CRREL, NP and SIMB3 ice buoys and the IceBridge flights respectively.

The median difference between the IST component and ECMWF-derived ice buoys (Figure 20) ranges between 0°C and -5°C for the Northern Hemisphere (a) and between -4°C and -2°C for the Southern Hemisphere (b) with no clear impact of the number of match-ups on the median difference values. The robust standard deviation is in the range 1°C to 4°C for both hemispheres. Statistics are similar for all other types of ice buoys (Figures 21-23) as expected, due to the difference in the measured quantity, i.e. ice buoys record air surface temperature typically at 2 m which has higher variability and is different to the surface skin temperature. Figure 24 shows the statistics against the IceBridge flights, available from 2012 to 2023, mostly for the Northern Hemisphere. Median differences are mostly positive, between 0°C and 2°C and the robust standard deviation ranges between 1.5°C and 3.5°C. This pattern is the opposite of that reported for the sea-ice buoys that record air temperature and indicates higher values for the IST component of the C3S L4 SST/IST dataset; it can be related to the fact that the IceBridge radiometer measures the radiometric surface temperature from an aircraft at an approximate height of 450 m above ground level (a.g.l.) without any cloud screening, and the presence of undetected clouds may explain the lower values in the IceBridge flights. Nonetheless, note that the median difference and robust standard deviation for these flights are the lowest compared to the statistics using the sea-ice buoys.

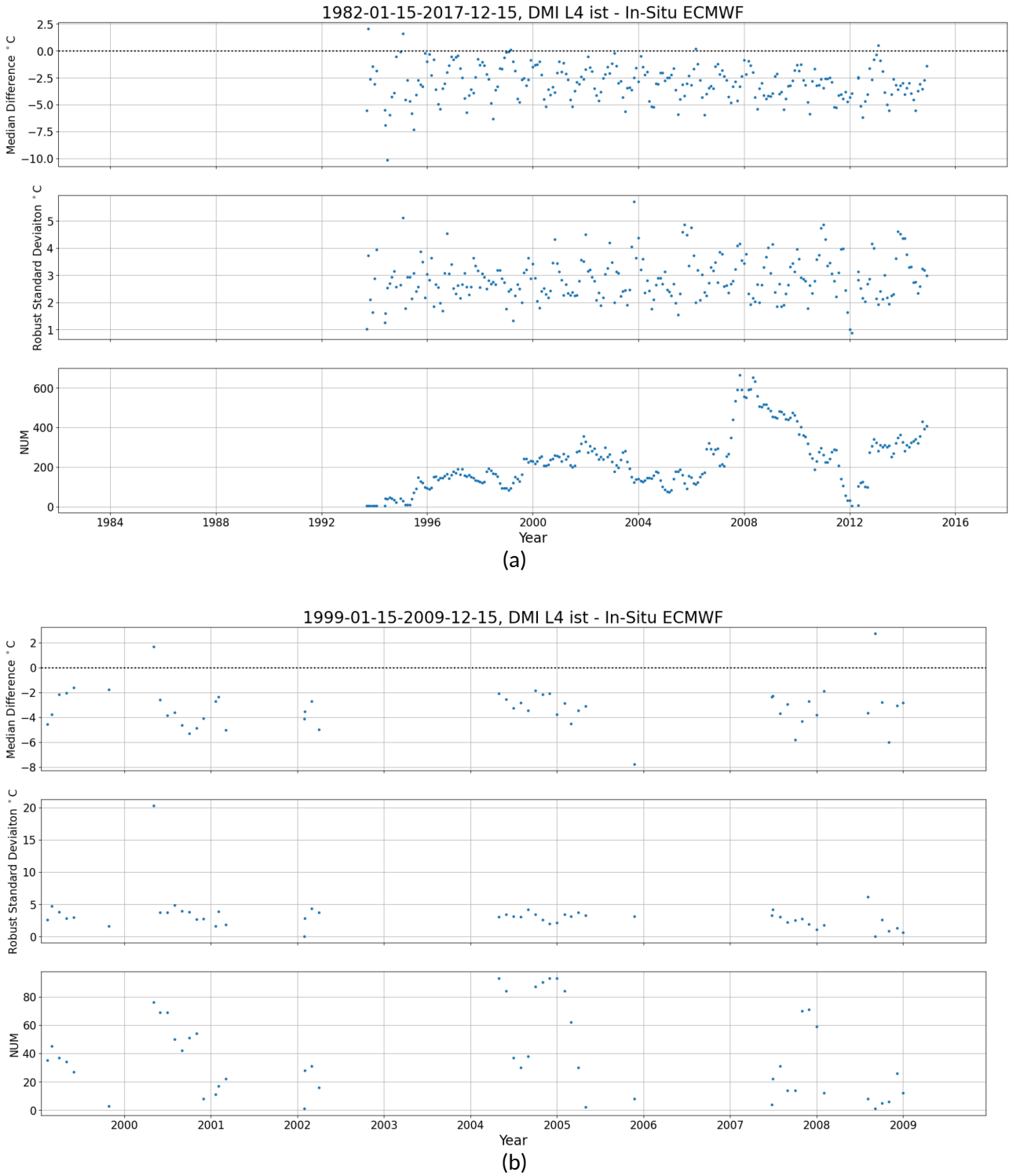

Figure 20. Time-series of IST median difference, robust standard deviation and number of match-ups between the SST/IST CDR v1.0 and ICDR v1.0 and ECMWF buoys for a) the Northern Hemisphere (NH) and b) the Southern Hemisphere (SH).

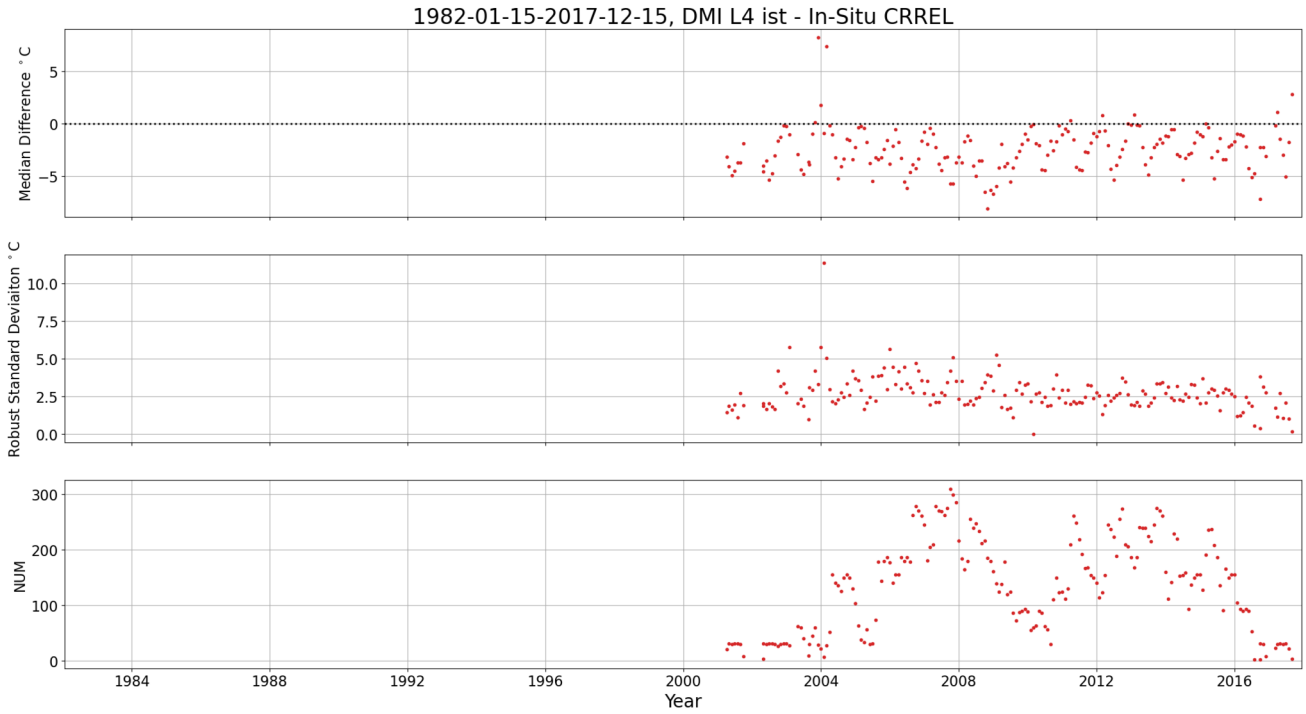

Figure 21. Time-series of IST median difference, robust standard deviation and number of match-ups between the SST/IST CDR v1.0 and ICDR v1.0 and the Northern Hemisphere CRREL buoys.

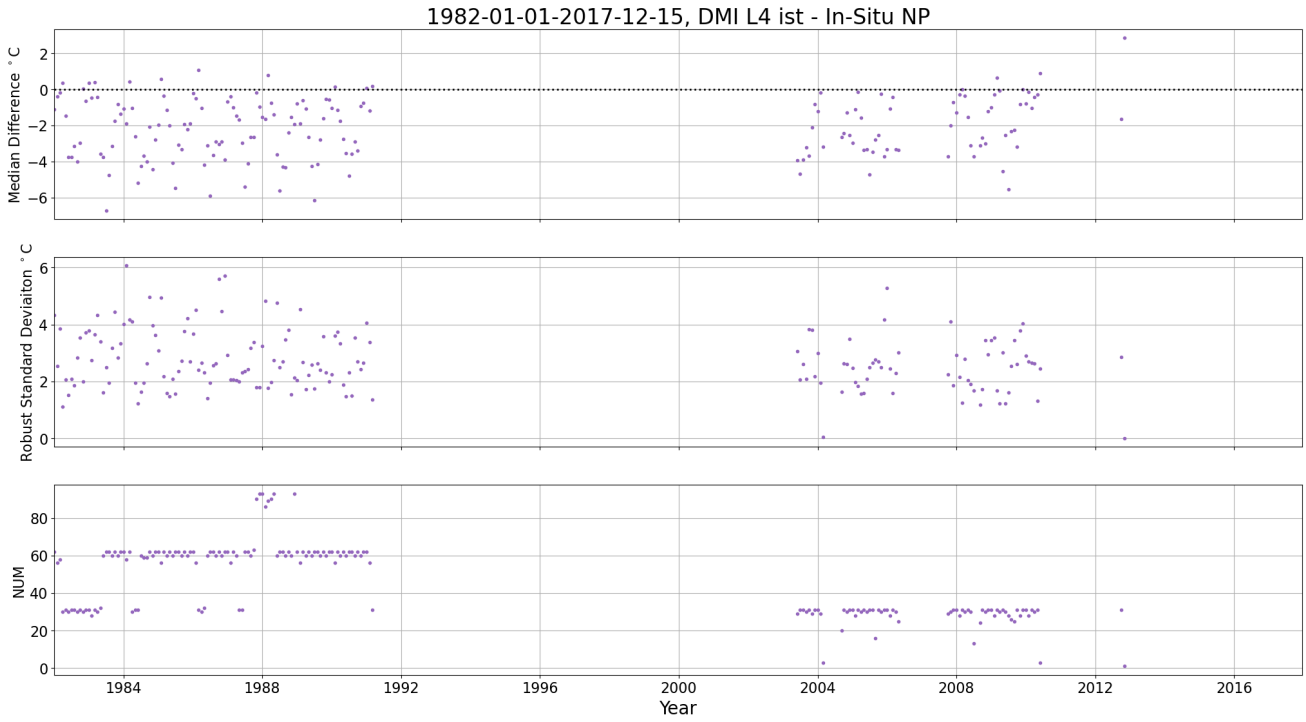

Figure 22. Time-series of IST median difference, robust standard deviation and number of match-ups between the SST/IST CDR v1.0 and ICDR v1.0 and the North Pole Drifting Ice Stations.

Figure 23. Time-series of IST median difference, robust standard deviation and number of match-ups between the SST/IST CDR v1.0 and ICDR v1.0 and the Northern Hemisphere SIMB3 buoys.

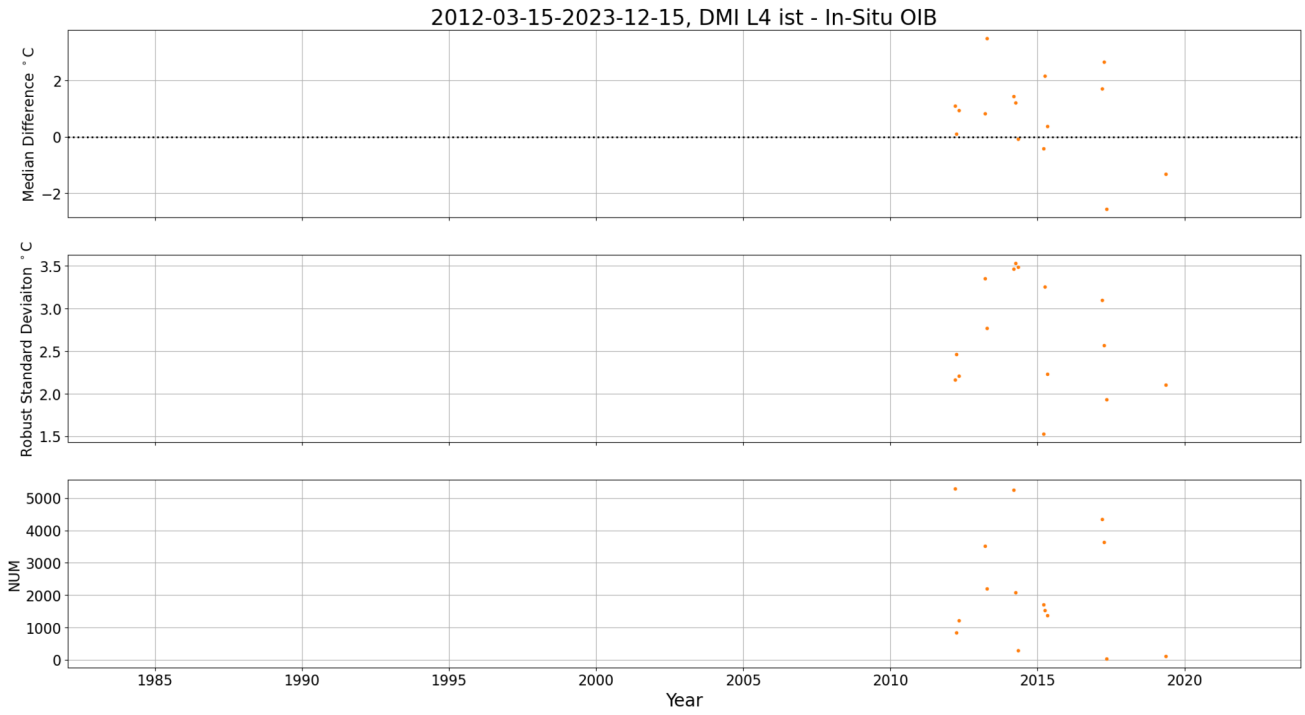

Figure 24. Time-series of IST median difference, robust standard deviation and number of match-ups between the SST/IST CDR v1.0 and ICDR v1.0 and IceBridge flights for the Northern Hemisphere (NH).

2.2.2 Spatial distribution

Figures 25 to 29 show the spatial distribution dependence of the (a) median difference, (b) robust standard deviation and (c) number of match-ups between the IST component of the SST/IST CDR/ICDR v1.0 and in situ observations from the ECMWF-derived, CRREL, NP and SIMB3 sea-ice buoys and IceBridge flights, respectively, for the Northern Hemisphere. The spatial availability of the match-ups is very limited for the South Hemisphere hence the plots are not shown. Match-ups are generally very limited which renders the proper validation of sea-ice surface temperatures more challenging. Median differences are mostly around 2 degrees, with higher values in the Beaufort Sea and east of Greenland, and more negative values in the central Arctic when ECMWF buoys are considered; which also show the lowest robust standard deviation values throughout the Arctic region and have most available match-ups.

CRREL, NP and SIMB 3 buoys (Figures 26 to 28) show similar patterns with positive median differences for most of the Arctic region, mostly uniform robust standard deviation and low number of available match-ups.

IceBridge flights (Figure 29) are constrained in the North American and European parts of the Arctic, showing highly positive median biases, robust standard deviation mostly below 1.5°C, and low numbers of match-ups.

(a)

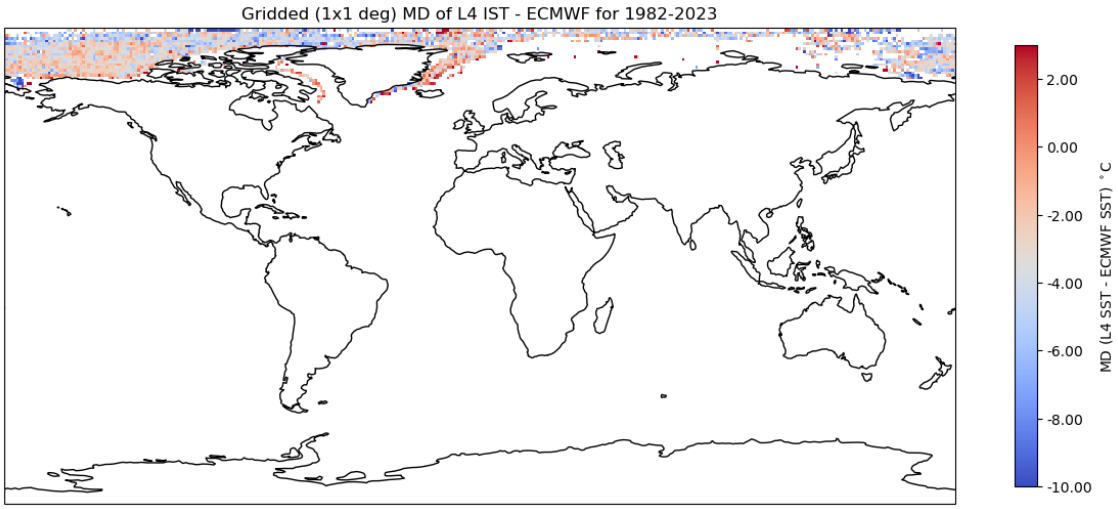

(b)

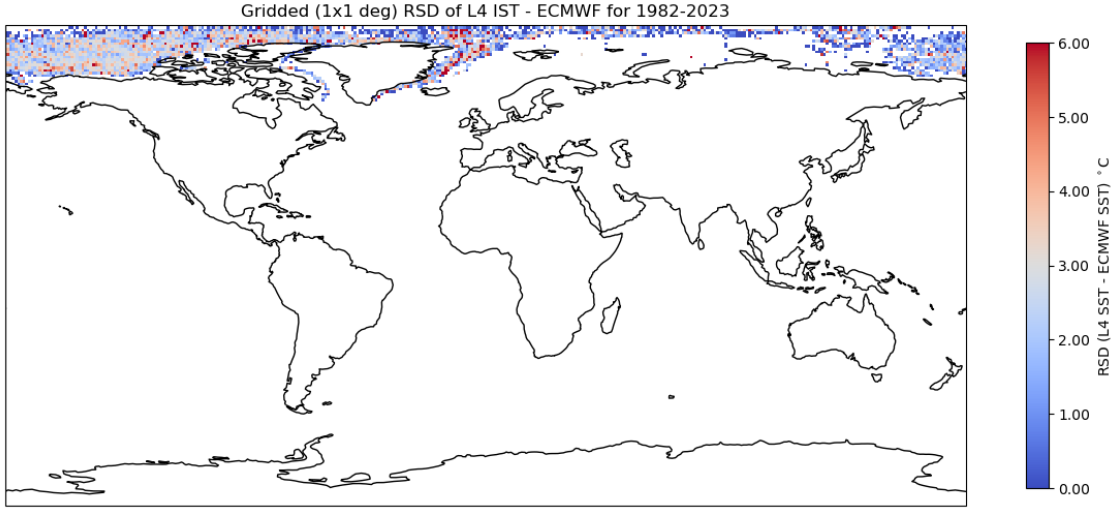

(c)

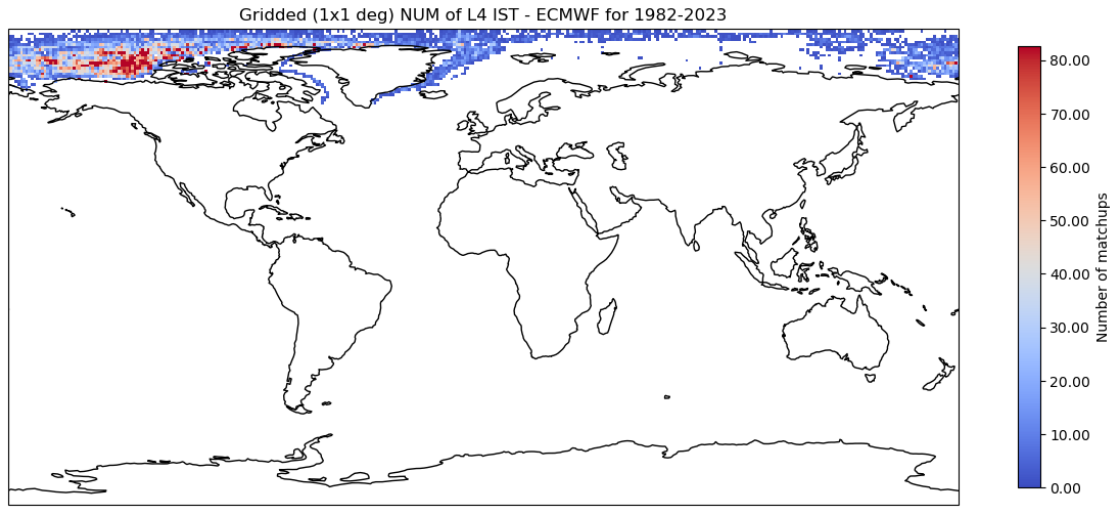

Figure 25. Spatial distribution of median difference (a), robust standard deviation (b) and number of match-ups (c) between the IST component of the SST/IST CDR/ICDR v1.0 and ECMWF buoys for the Northern Hemisphere.

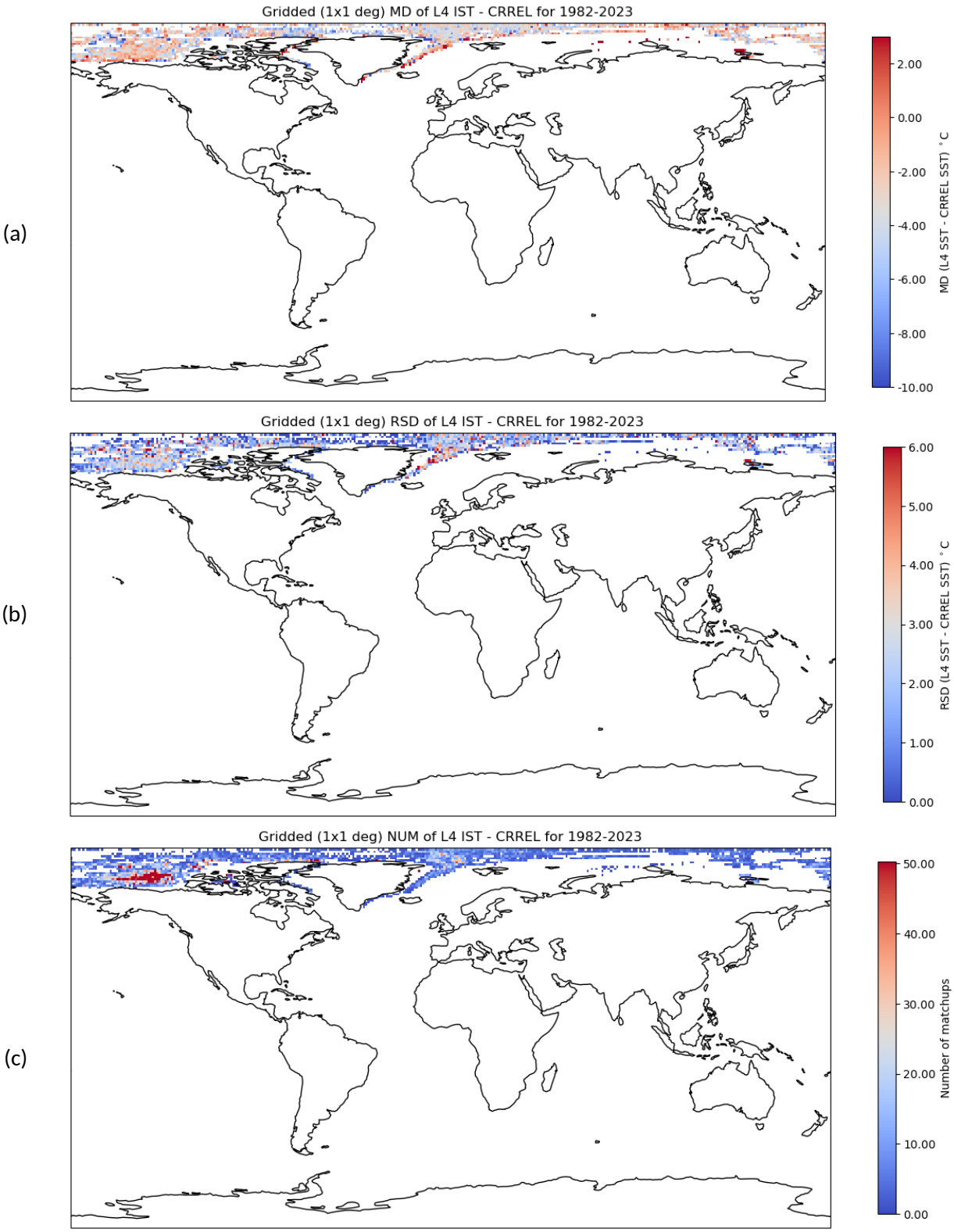

Figure 26. Spatial distribution of median difference (a), robust standard deviation (b) and number of match-ups (c) between the IST component of the SST/IST CDR/ICDR v1.0 and the Northern Hemisphere CRREL buoys.

(a)

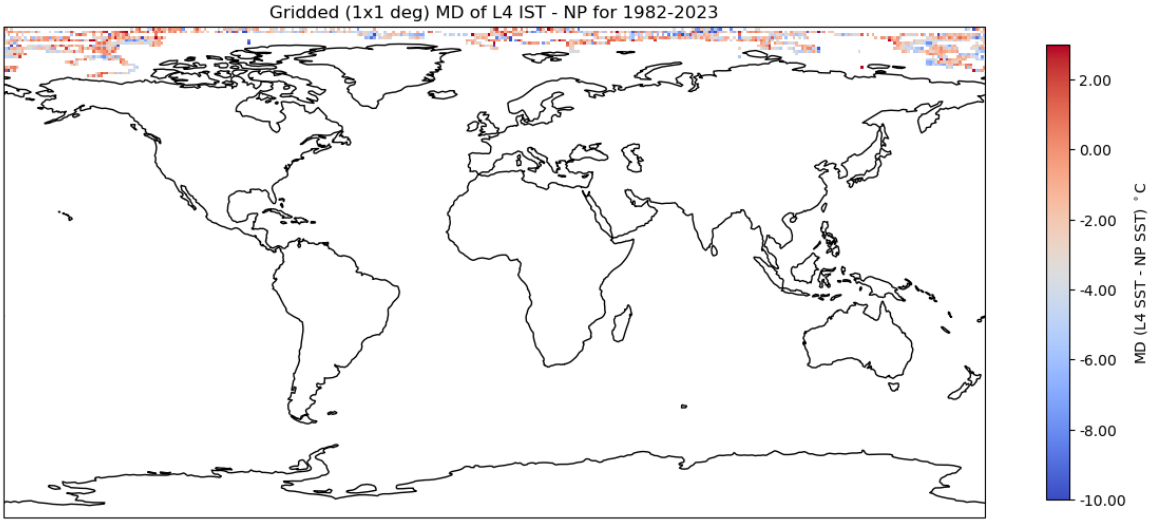

(b)

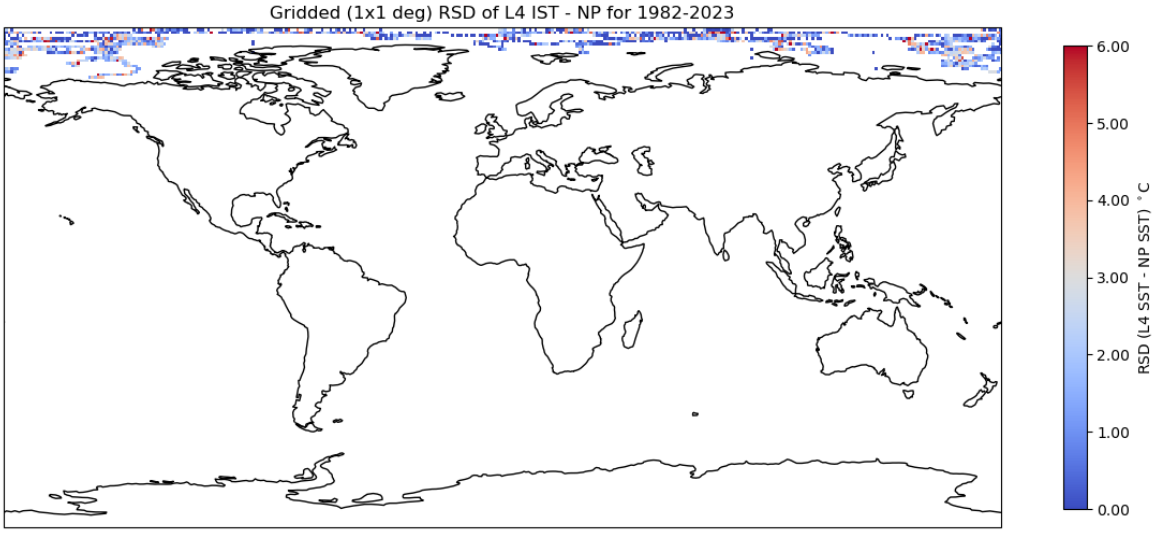

(c)

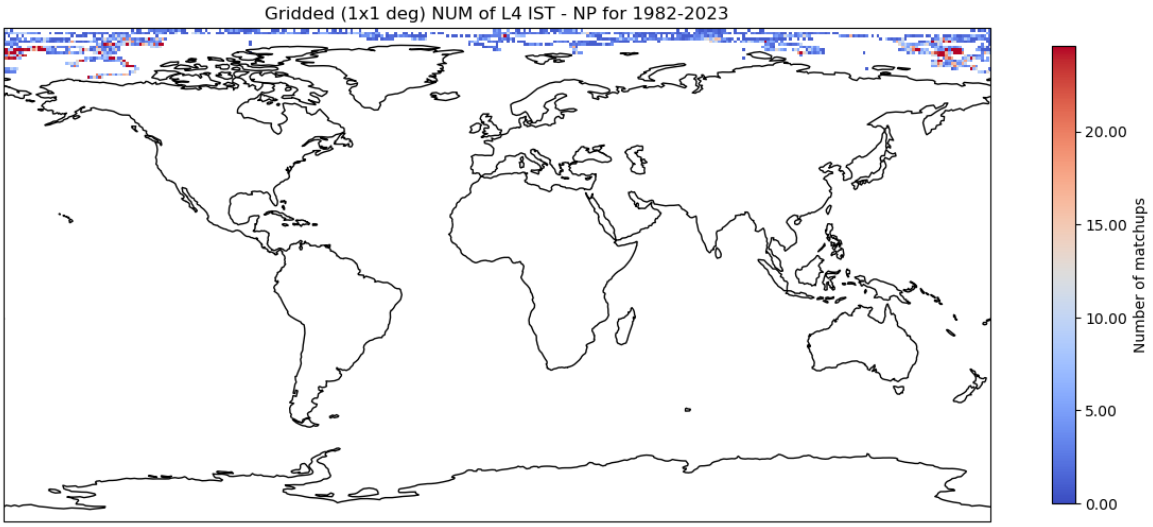

Figure 27. Spatial distribution of median difference (a), robust standard deviation (b) and number of match-ups (c) between the IST component of the SST/IST CDR/ICDR v1.0 and the North Pole Drifting Ice buoys.

(a)

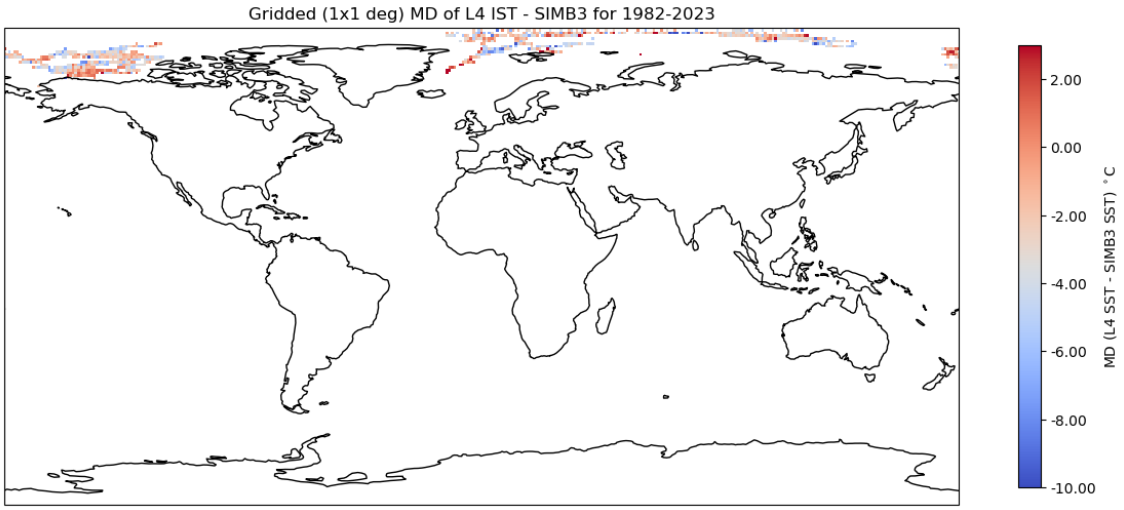

(b)

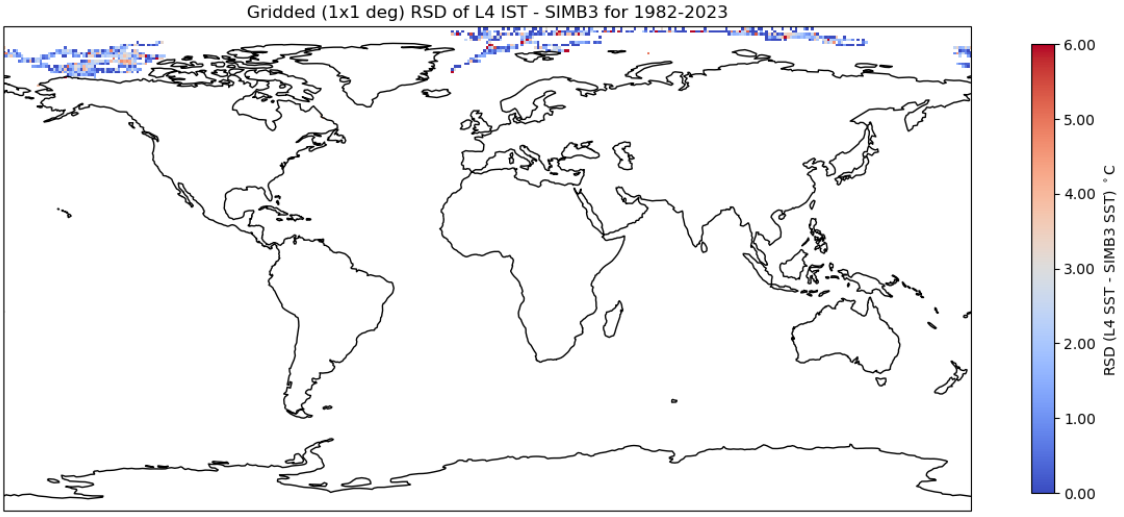

(c)

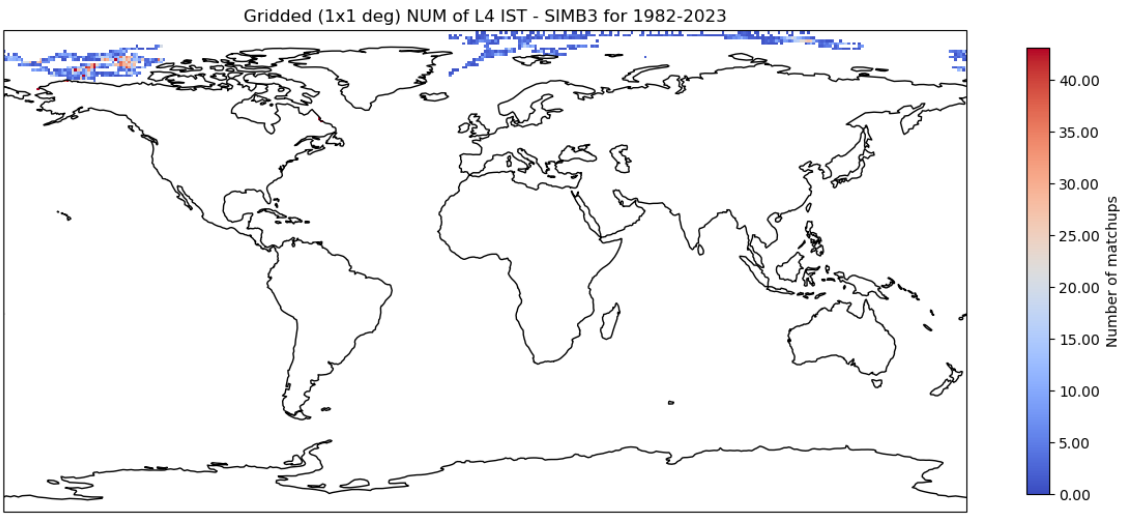

Figure 28. Spatial distribution of median difference (a), robust standard deviation (b) and number of match-ups (c) between the IST component of the SST/IST CDR/ICDR v1.0 and the Northern Hemisphere SIMB3 buoys.

(a)

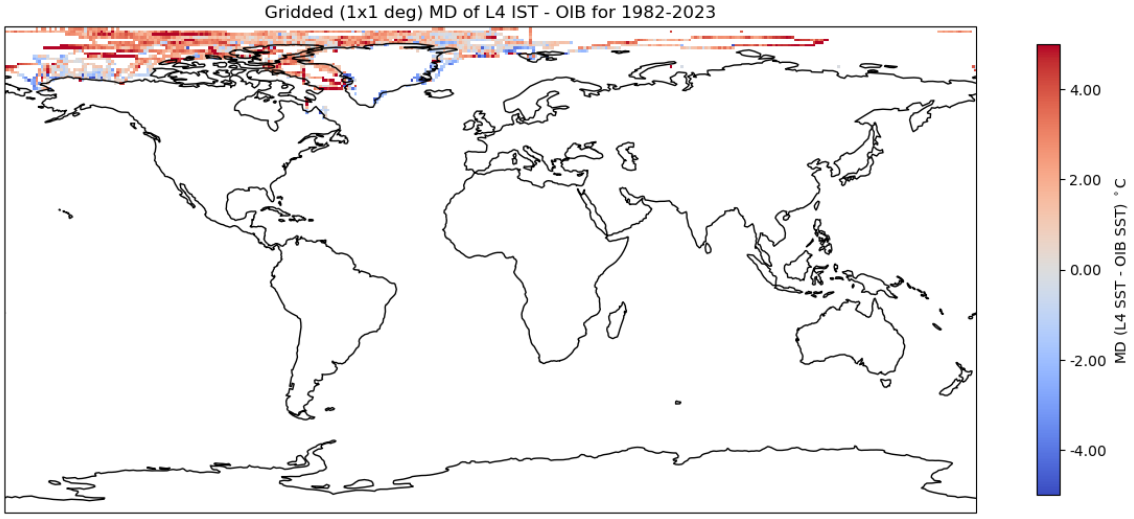

(b)

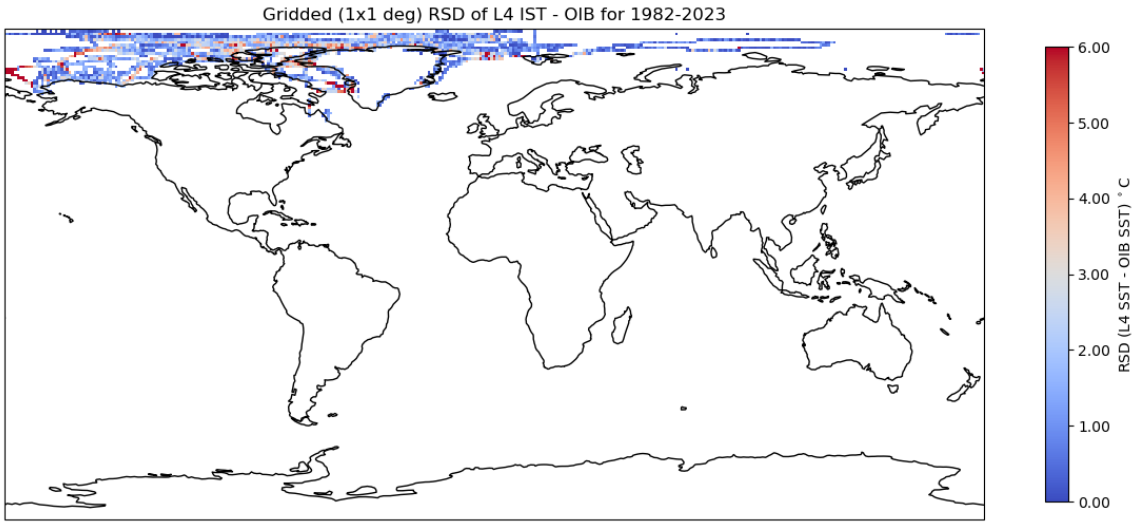

(c)

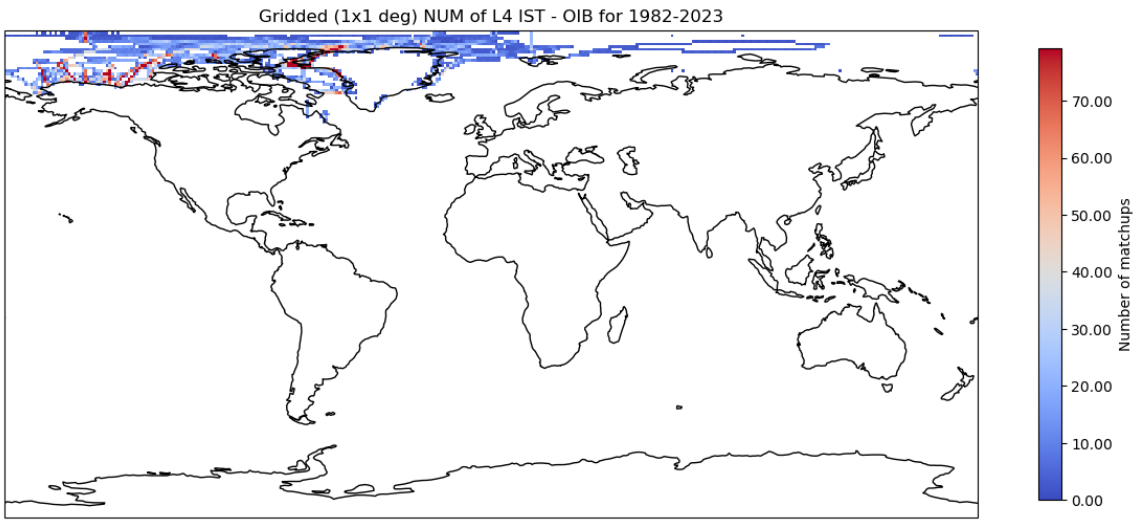

Figure 29. Spatial distribution of median difference (a), robust standard deviation (b) and number of match-ups (c) between the IST component of the SST/IST CDR/ICDR v1.0 and IceBridge flights for the Northern Hemisphere.

2.2.3 Histogram distribution

Figure 30 shows the histogram distribution of median bias between the IST component of the C3S Global L4 SST/IST product and in situ observations from ECMWF obtained sea ice buoys for (a) the Northern Hemisphere and (b) the Southern Hemisphere. Figure 31 shows the histogram of median bias between the IST component of the C3S Global L4 SST/IST product and in situ observations from (a) CRREL buoys and (b) North Pole Ice stations for the Northern Hemisphere. Figure 32 shows the histogram of median bias between the IST component of the C3S Global L4 SST/IST product and in situ observations from SIMB3 buoys in the Northern Hemisphere while the histograms derived from IceBridge flights for (a) the Northern and (b) the Southern Hemisphere are shown Figure 33.

For all sea ice buoy stations that report air temperature, the histograms are typically skewed towards negative values, indicating higher in situ temperatures. They also demonstrate that there are few, extreme occurrences that reach to more than 10° while they are not smooth, due to the limited number of match-ups available. This is the case in both hemispheres, as seen from the ECMWF buoys in Figure 30 (a and b).

For the IceBridge flights, that record surface skin temperature and are thus directly comparable with the IST component of the C3S Global L4 SST/IST product, in the Northern Hemisphere, shown in Figure 33 (a) the opposite occurs, i.e. the histogram is skewed to the right indicating higher C3S Global L4 SST/IST values. This can be related to the fact that the IceBridge radiometer measures the radiometric surface temperature from an aircraft at an approximate height of 450 m a.g.l. without any cloud screening, and the presence of undetected clouds may explain the lower values in the IceBridge flights. Nonetheless, the median difference and robust standard deviation for these flights are lower than those calculated using the sea-ice buoys. For the Southern Hemisphere IceBridge flights, shown in Figure 33 (b), there only a few available flights (four) and no meaningful statistics can be derived.

(a)

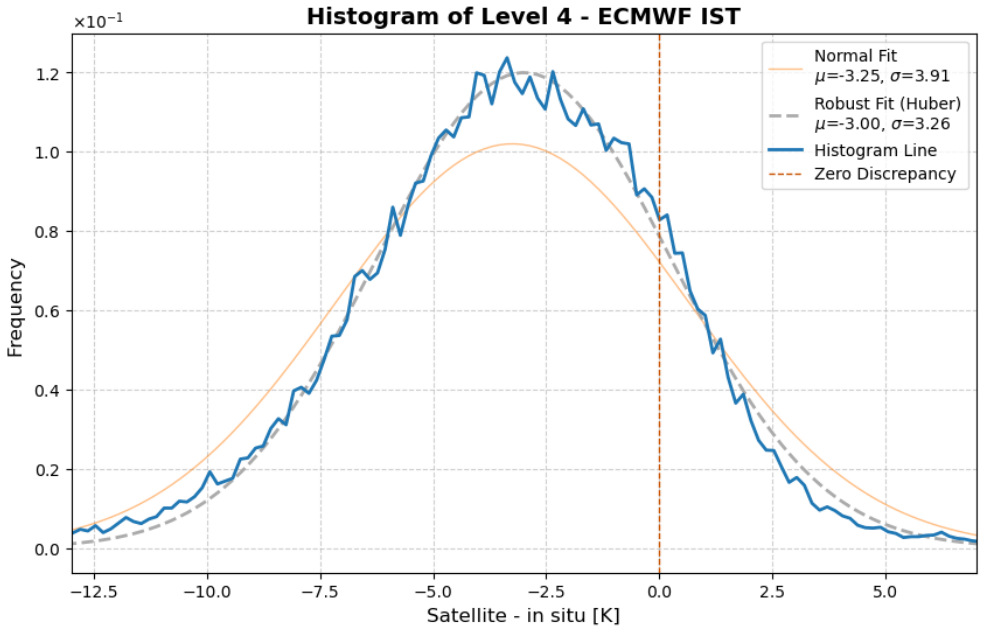

(b)

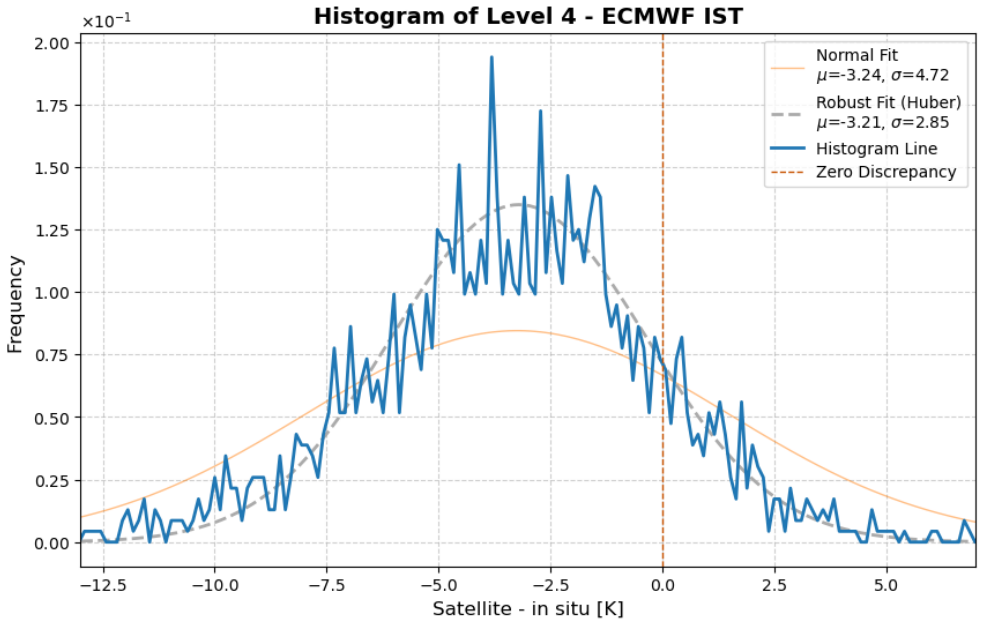

Figure 30. Histogram distribution of differences between the IST component of the SST/IST CDR/ICDR v1.0 and ECMWF buoys for a) the Northern and b) Southern Hemisphere.

(a)

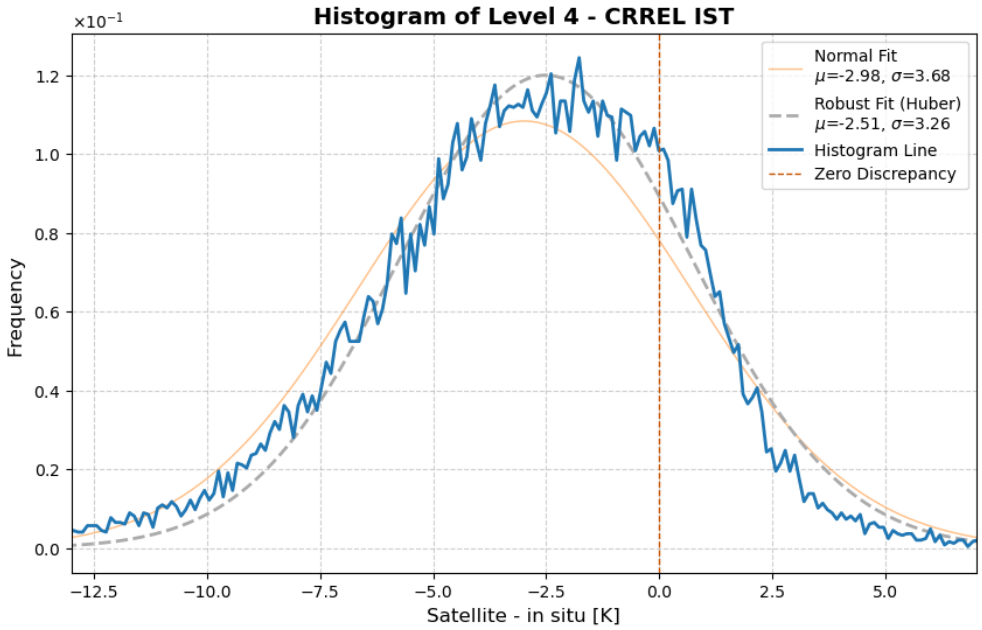

(b)

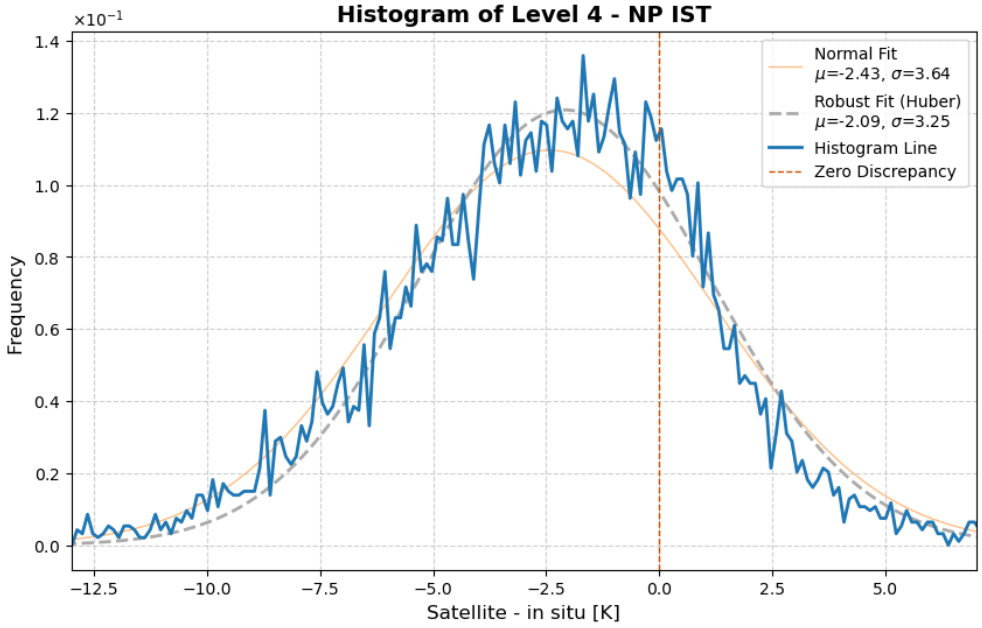

Figure 31. Histogram distribution of differences between the IST component of the SST/IST CDR/ICDR v1.0 and a) the Northern Hemisphere CRREL buoys, and b) the North Pole Drifting Ice buoys.

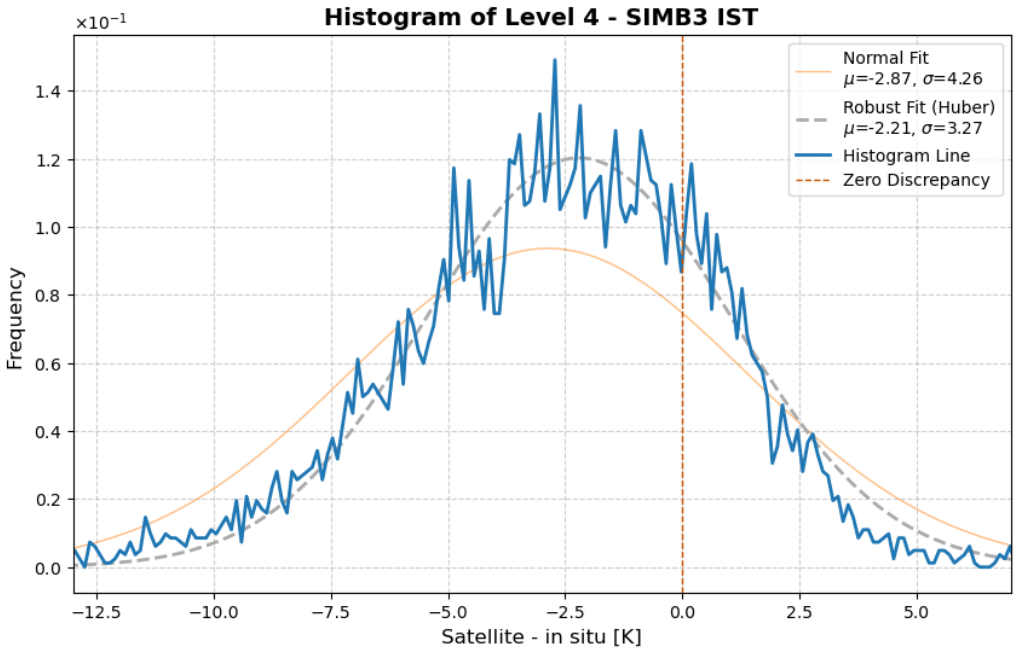

Figure 32. Histogram distribution of differences between the IST component of the SST/IST CDR/ICDR v1.0 and the Northern Hemisphere SIMB3 buoys.

(a)

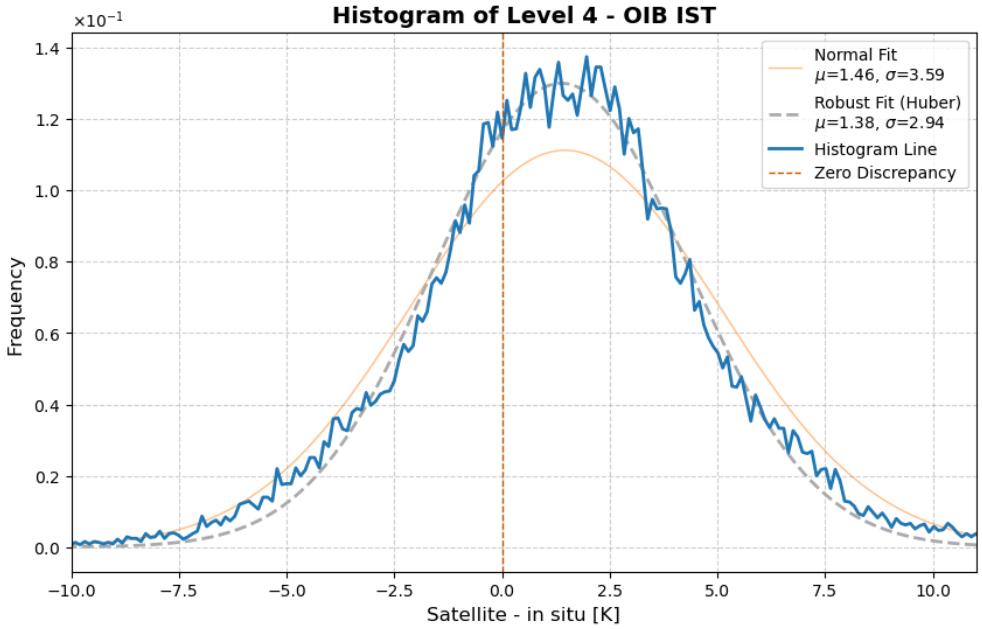

(b)

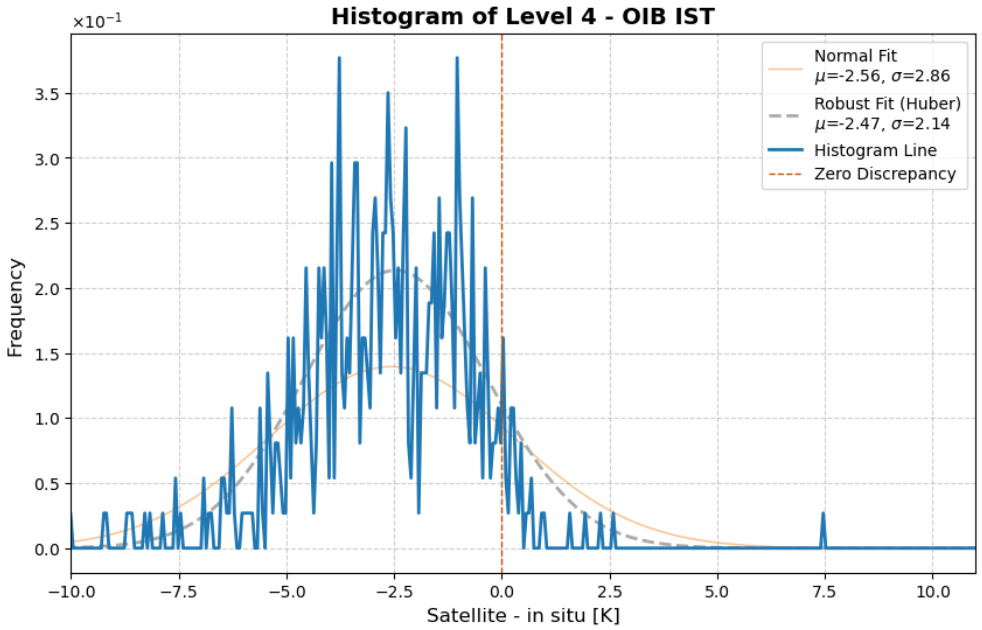

Figure 33. Histogram distribution of differences between the IST component of the SST/IST CDR/ICDR v1.0 and IceBridge flights for a) the Northern and b) Southern Hemisphere.

2.3 Spectral Analysis

To assess the effective spatial resolution of the L4 SST/IST product in terms of the spatial scales resolved, six sub-domains (regions) covering the major ocean basins (North and South Atlantic, North, South and Tropical Pacific, Indian Ocean) were identified in the global ocean between 60°S and 60°N, shown in Figure 34. Ten random years were selected, i.e. 1987, 1988, 1996, 1997, 2009, 2010, 2018, 2019, 2022 and 2023, to cover the different periods of satellite data availability from the earlier years with less sensors to the more recent years with more sensors. For each sub-domain, spectra were calculated daily using a Fast Fourier Transform (FFT)[3] and then averaged for the entire period of investigation. This is a common method to assess the effective spatial resolution of gridded datasets, either model-based or from satellite data, and can inform on the length-scales represented in the datasets and their effective spatial resolution (Karagali et al., 2013; Castro et al., 2017; Nielsen-Englyst et al., 2024).

Figure 35 shows the latitudinally averaged spectra for the six sub-domains as computed from the Global L4 SST/IST dataset (black solid lines, DMIOI) and the latest version (v3.0) of the ESA SST_cci Global L4 SST Analysis (gray lines, OSTIA) for reference. The black dashed lines are the theoretical curves for the -5/3 and -2 slopes, which spectra are expected to follow in the meso-scale, i.e. between 2km and 200 km. This is generally the case for both products. Spectral power is at the same level for both the C3S Global L4 SST/IST product and the ESA SST_cci Global L4 SST Analysis for length scales between 628 km and 60 km, in all sub-domains. Nonetheless, for scales between 60 km and 10 km, i.e. double the grid spacing of both products, the C3S Global L4 SST/IST product maintains a higher spectral power and shows a smoother decrease for smaller length scales when

[3] See https://en.wikipedia.org/wiki/Fast_Fourier_transform [last accessed March 19, 2025]

compared to the ESA SST_cci Global L4 SST Analysis, which shows a sudden drop of spectral power at 60 km. The maintenance of higher spectral power for length scales smaller than 60 km for the C3S Global L4 SST/IST product indicates that the representative features of such length-scales are resolved and thus contribute to the spectral energy. When features of certain length scales are not resolved, the spectral power at these length scales decreases.

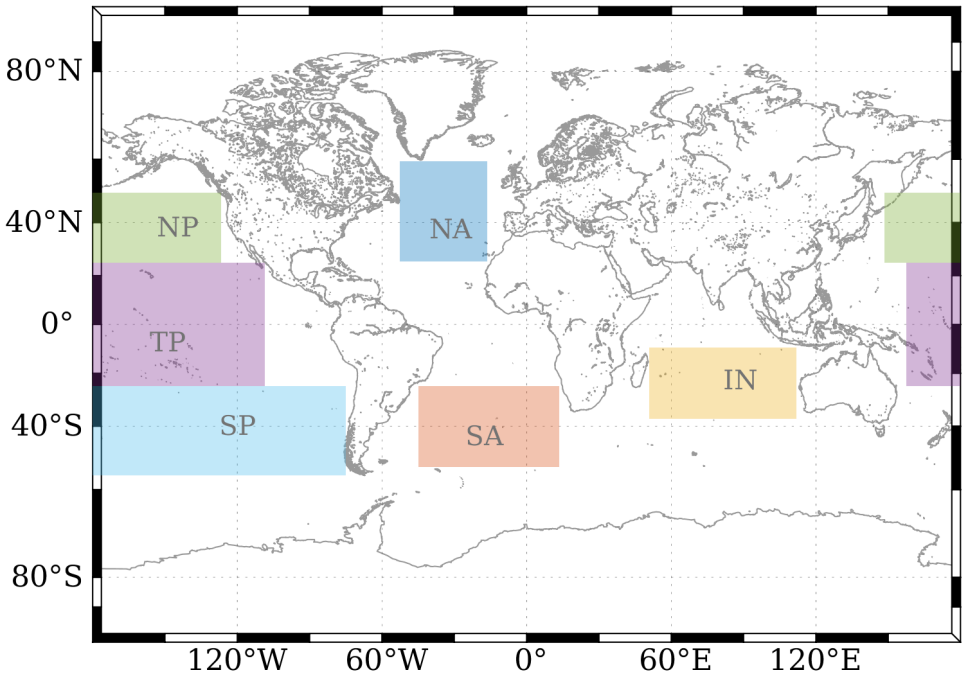

Figure 34. The six sub-domains used for the spectral analysis: North Pacific (NP) in green, Tropical Pacific (TP) in magenta, South Pacific (SP) in light blue, North Atlantic (NA) in dark blue, South Atlantic (SA) in orange and Indian Ocean (IN) in yellow.

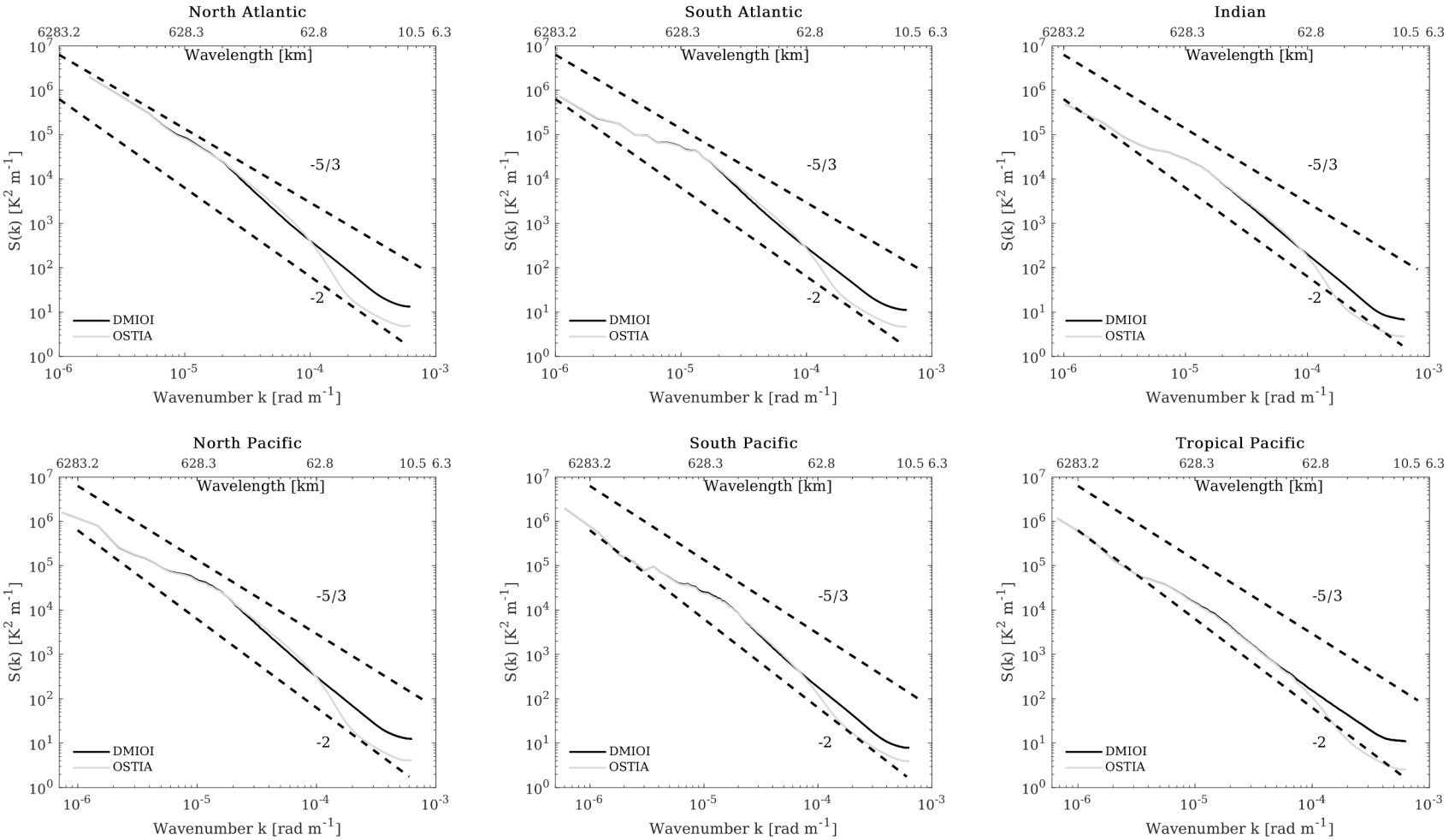

Figure 35. Latitudinal spectra for the six sub-domains: NA, SA, IN (top row) and NP, SP, TP (bottom row). The black solid lines represent the spectra derived from the Global L4 SST/IST dataset, the dashed black lines are the theoretical curves for -5/3 and -2 slopes (typically expected in the meso-scale region) and the gray line is the spectra calculated from the ESA SST_cci Global L4 SST Analysis product (v3.0) for the same sub-domains and following the same methodology.

2.4 SST Uncertainty validation

Uncertainty validation plots for the SST component using the in situ observations from the drifting buoys are shown in Figure 36. The dashed lines represent the ideal uncertainty based on the assumption that drifters have a total uncertainty of 0.2 K (Kennedy, 2014).

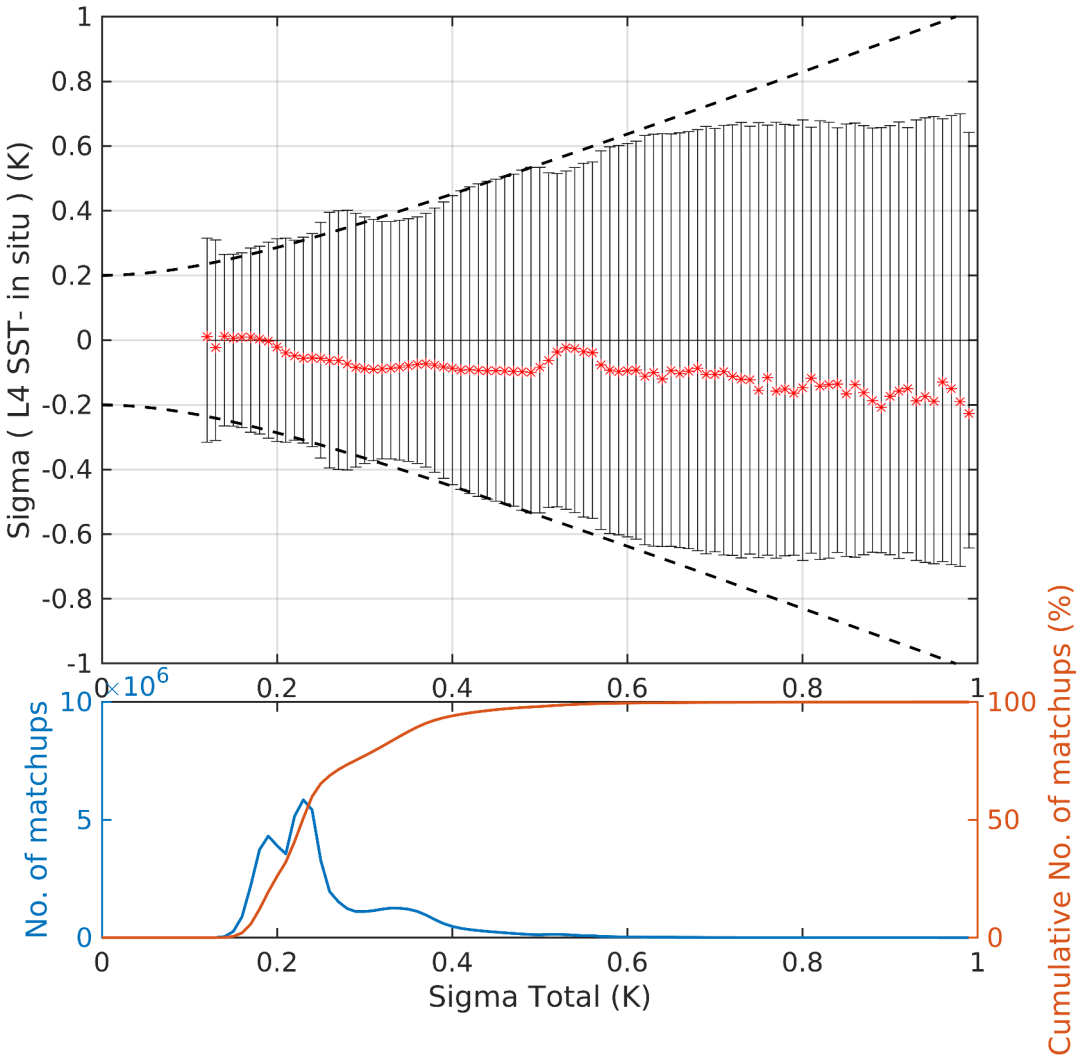

Figure 36. Uncertainty validation of SST using drifting buoys. Along the x-axis is the estimated uncertainty which is calculated as part of the Optimal Interpolation (OI). The y-axis represents the standard deviation between the L4 SST and in situ measurement, which will be affected by errors in both the satellite and in situ observations. The dashed lines show the ideal uncertainty when accounting for uncertainties in the drifter SSTs and the sampling error. The solid black lines show one standard deviation of the L4 SST minus drifter SST differences for each 0.02 K bin and the red asterisks mark the mean difference. The bottom plots show the number of matchups (blue) and the cumulative percentage of matchups for each bin (red).

2.5 IST Uncertainty assessment

Unlike the case of SST, uncertainties for the IST component could not be validated due to lack of long-term reference measurements of surface skin temperature over the sea ice. Instead, an uncertainty assessment could be performed on the IST uncertainties of the L4 SST/IST dataset versus time. These are separated into uncertainties for the Marginal Ice Zone (MIZ) and for the sea-ice (IST) and are shown in Figure 37 seasonally, by applying 3-month moving means (a), and as monthly means (b) over the entire CDR and ICDR period.

The MIZ uncertainties are higher due to the more variable nature of the MIZ, a mix of open water and sea-ice that changes in size depending on the year. Nonetheless, the MIZ uncertainties appear relatively stable throughout the CDR/ICDR record (Figure 30a) while a seasonal cycle is also present with higher uncertainties in spring and autumn (of the Northern Hemisphere, where most of the MIZ is present) during when most of the melting/formation of sea-ice occurs.

The IST uncertainties (blue) are lower and show higher seasonal variability throughout the CDR/ICDR record. Their annual cycle indicates uncertainties being lowest in April (which is typically around the end of the maximum sea-ice extend and about when melting starts in the Northern Hemisphere) and highest between September and October (when typically sea-ice extend is minimum and just before freezing starts).

(a)

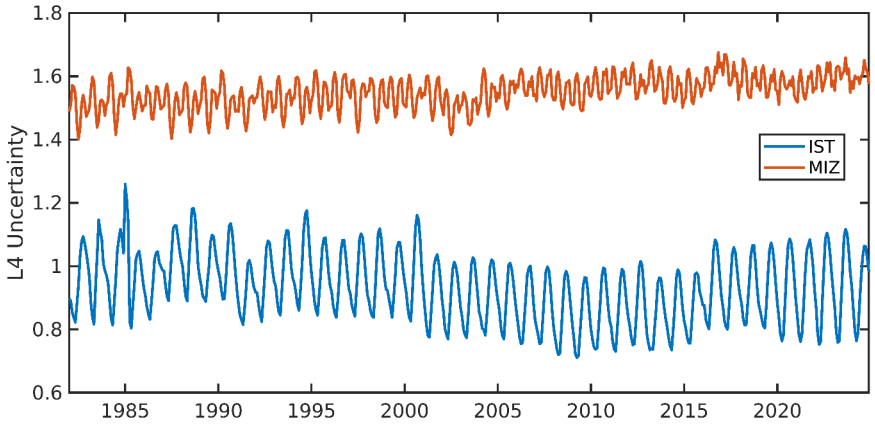

(b)

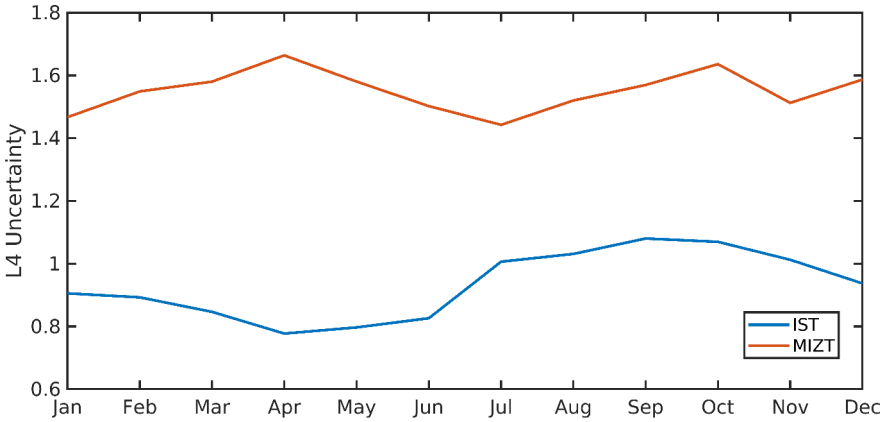

Figure 37. Uncertainty assessment of the IST component (blue), including the Marginal Ice Zone (MIZ, red), of the SST/IST CDR/ICDR v1.0 for the period 1982-2024.

2.6 Stability Assessment

The stability of the CDR is assessed separately for the SST and IST components, and results are shown in Table 3. As per [D6], the requirements of an SST CDR are a goal measurement uncertainty of 0.05 K and a goal stability (per decade) of 0.01 K according to WMO (2022). Both requirements are met for the SST component of the L4 SST/IST CDR/ICDR.

For the Ice Surface temperature, the CDR requirements are 0.3 K/decade for the threshold stability and 0.1 K/decade for the target stability (WMO, 2022). Accuracy requirements are presented as measurement uncertainties (2-sigma), with threshold values of 6 K, breakthrough values of 3 K and goal values of 1 K. The stability requirement is well met for the IST component and the accuracy requirement is somewhat higher that the breakthrough values. Nonetheless it should be kept in mind that for the IST, statistics are calculated using in situ observations from stations that report air temperatures rather than surface skin temperatures and such deviations are expected.

Table 3. Relative trend between the L4 SST and IST components and selected long-term stable in situ measurements from drifting buoys (SST) and ECMWF distributed drifting ice buoys, CRREL and NP buoys (IST). For the South Hemisphere (SH) IST accuracy and stability assessment only ECMWF distributed drifting ice buoys were used. Results are calculated for the period 1982-2023.

Type	Threshold Relative Trend (Stability)	Goal Relative Trend (Stability)	Achieved Relative Trend (Stability)	Threshold Accuracy	Goal Accuracy	Achieved Accuracy
SST	0.1 K/decade	0.01 K/decade	-0.009±0.0021 °C/dec	0.3 K	0.05 K	-0.04 °C
IST NH (SH)	0.3 K/decade	0.1 K/decade	-0.061±0.067 (0.006±0.73) °C/dec	6 K	1 K	-2.60 (-3.24) °C

3. Application(s) specific assessments

Climate assessment, i.e. a detailed assessment of trends and variability in the L4 SST/IST CDR and ICDR (including year 2024), was performed relative to the 1991-2020 climatology. The monthly (blue line) and annual anomalies (red line) from the climatology are shown in Figure 38 where an overall positive trend of 0.0118±0.0003 °C/yr (0.118 °C/decade) is identified, amounting to a total global combined sea and sea-ice surface temperature warming of 0.5 °C during the period of 42 years from 1982 to 2024.

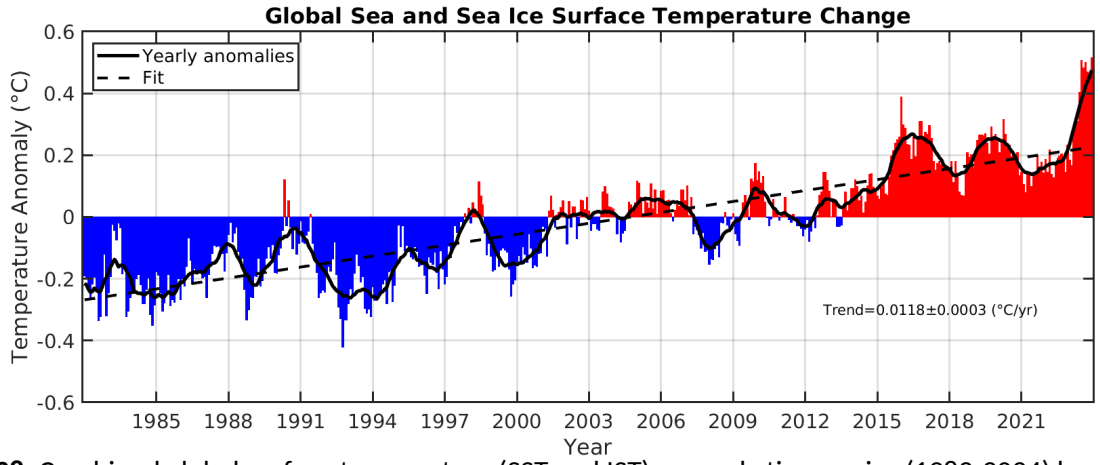

Figure 38. Combined global surface temperature (SST and IST) anomaly time-series (1982-2024) based on SST/IST CDR v1.0 and ICDR v1.0. The vertical bars indicate the monthly anomalies below (blue) or above (red) zero relative to the CDR1.0 climatology, which is the average of the period 1991 – 2020.

When only the region between 60° South and North is considered, thus sea-ice covered areas are mostly excluded (note there could still be some sea-ice lower of 60 ° North for some periods of some years), the combined global surface temperature anomalies from 1982 to 2024 are shown in Figure 39, with an estimated trend of 0.0091±0.0003°C/year (0.091 °C/decade), amounting to a total surface temperature warming of 0.38 °C during the period of 42 years, i.e. 25% lower than the global combined surface temperature including the polar regions (see Figure 38). This highlights the importance of including sea surface and sea-ice surface temperature when estimating surface temperature trends.

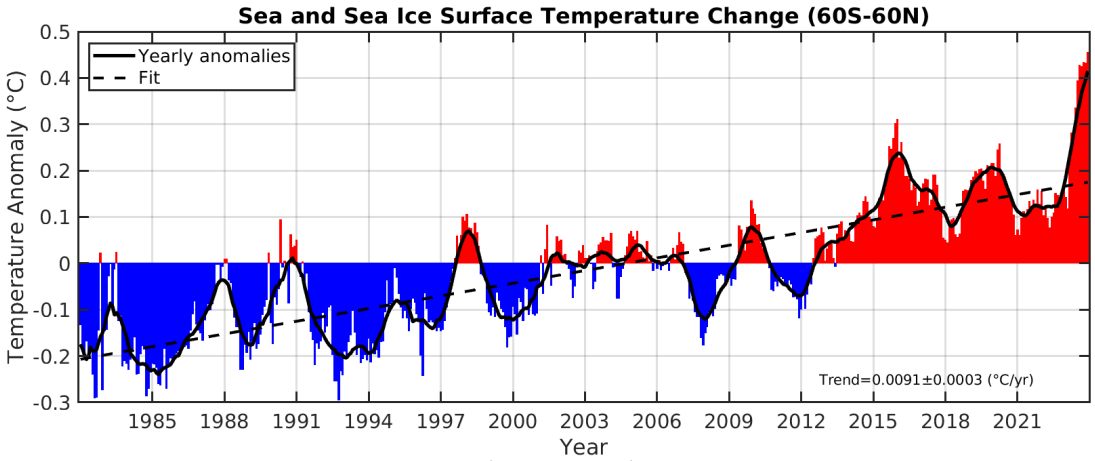

Figure 39. Combined global surface temperature (SST and IST) anomaly time-series based on SST/IST CDR v1.0 and ICDR v1.0, confined to the region between 60 degrees South and 60 degrees North. The vertical bars indicate the monthly anomalies below (blue) or above (red) zero relative to the CDR1.0 climatology, which is the average of the period 1991 – 2020.

3.1 Known issues

Issues reported below are associated with the input datasets used to create the DMI-MSC-SIC product which is used as a mask to characterize open water surfaces and sea-ice surfaces in the dataset. Once categorised, open water pixels are assigned an SST value; fully sea-ice covered areas are assigned an IST value, while the marginal ice zone areas are assigned a weighted value between SST and IST see [D4].

Issue with Ice Charts. An input to the DMI-MSC-SIC product, the sea ice charts for December 1987 and January 1988 have been found to have a high uncertainty, particularly in the Southern Hemisphere. This was assessed visually and there is no means of confirmation, therefore the DMI-MSC-SIC sea ice concentration field included in the daily files of the C3S Global L4 SST/IST product should be used with caution for the stated period and region. Note that this does not extend to the accompanying SST and IST values for the same period.

Issue with SIC from OSI-450-a. An error randomly appearing on 343 days throughout the 40-year span of the satellite-derived SIC data in the OSI-450-a product, was announced in September 2024[4]. This was associated with a filter adjusting for land-spillover effects. For the L4 SST/IST CDR/ICDR (i) only 60 days from the 343 are relevant (this OSI-450-a product was only used for the 1982 to 1991 period, see section 3.4 in [D4]), and (ii) as the SIC is only used as a mask, the issue has minimal to no impact on the L4 CDR/ICDR. Therefore, any SIC information contained in the L4 SST/IST CDR/ICDR stemming from the OSI-450-a product, uses the old faulty information and not the updated files released after September 2024, which users must keep in mind when looking at the SIC mask over the affected period.

[4] See https://osisaf-hl.met.no/patch-osi-450-a (last accessed 03/03/2025)

4. Compliance with user requirements

User requirements are listed in D5 and are reproduced below with the corresponding levels achieved by the product. In this section, each property is assessed against the requirements outlined by GCOS (WMO, 2022). Requirements are on an ascending scale, with:

- **Threshold requirements**, representing the minimum acceptable level for climate monitoring;
- **Target requirements**, representing the desired level that provides reliable and useful data;
- **Goal requirements**, representing the idea level to maximise understanding and predictive capabilities.

4.1 Definitional requirements

Property	Threshold	Target	Status
SST at 20 cm	Daily analysis of SSTs from multiple sensors	Daily analysis of SSTs from multiple sensors using proven methods to adjust observations to daily-mean at 20 cm	Target Achieved
IST at skin	Daily analysis of IST from at least 1 sensor	Daily analysis of IST from sensors using proved methods to derive sea-ice surface skin temperature	Target Achieved
Time	UTC	Standard time averaging or reporting time.	Target Achieved (12:00)

4.2 Coverage requirements

Property	Threshold	Target	Status
Gap-free analysis	Provide		Threshold Achieved
Spatial Coverage	Global	Global	Target Achieved
Temporal coverage	20 years	>40 years	Target Achieved
Sea-ice	Report a sea-ice surface temperature value (IST) and an SST value		Target Achieved

4.3 Spatial and temporal resolution requirements

Property	Threshold	Target	Status
Spatial resolution	0.1 degrees	0.05 degrees	Target Achieved
Spectral content	Document		Threshold Achieved
Temporal resolution	Daily	Daily	Target Achieved

4.4 Uncertainty requirements

4.4.1 Communication requirements

Property	Threshold	Target	Status
Standard uncertainty	Provide		Threshold Achieved
Quality indicators	Provide		Not provided A per datum, and simple-to-use confidence in uncertainty estimate is a required indicator. However, to-date, there is no direct quality indicator for uncertainty available. See sections 2.4 and 2.5 of this document, on uncertainty validation.
Validate uncertainty	Document		Threshold Achieved

4.4.2 Data uncertainty requirements

Property	Threshold	Target	Status
SST systematic uncertainty	0.1 K	0.1 K	Target achieved Uncertainty (bias) has been estimated over scales currently in the order of 100 km.
IST systematic uncertainty	2.5 K	1.5 K	Threshold achieved Uncertainty (bias) has been estimated over scales currently in the order of 100 km
SST Trend uncertainty	0.1 K/decade	0.01 K/decade	Target achieved This refers to stability within SST uncertainty, see Table 3.
SST annual stability	0.1 K	0.1 K	Target Achieved This refers to the maximum change of bias throughout the annual SST cycle at a given location
IST Trend uncertainty	0.03 K/yr	0.01 K/yr	Target achieved This refers to stability within IST uncertainty, see Table 3.

4.5 Format requirements

Property	Threshold	Target	Status
NetCDF, CF conventions	Provide	GHRSST GDS2.0	Target Achieved
Grid definition	Regular lat/lon		Threshold Achieved
Metadata community standards satisfied		GHRSST GDS2.0	Target Achieved
Traceable input and processing	Document		Threshold Achieved
Documentation	With data		Threshold Achieved Documentation is provided alongside the data on the data download site
Access and download	Free	Access tools and fast download	Target Achieved

4.6 Timeliness requirements

Property	Threshold	Target	Status
Timely updates	12 months	3 months	Threshold Achieved

References

Alerskans, E., Høyer, J.L., Gentemann, C.L, Pedersen, L.T., Nielsen-Englyst, P., and Donlon, C. (2020), Construction of a climate data record of sea surface temperature from passive microwave measurements, Remote Sens. Environ., 236, 111485, doi:10.1016/j.rse.2019.111485

Atkinson, C. P., Rayner, N. A., Kennedy, J. J., and Good, S. A. (2014), An integrated database of ocean temperature and salinity observations, J. Geophys. Res. Oceans, 119, 7139–7163, doi:10.1002/2014JC010053.

Castro, S. L., Emery, W. J., Wick, G. A., & Tandy, W. (2017). Submesoscale Sea Surface Temperature Variability from UAV and Satellite Measurements. Remote Sensing, 9(11), 1089. https://doi.org/10.3390/rs9111089

Karagali, I., Larsén, X. G., Badger, M., Peña, A., & Hasager, C. B. (2013). Spectral Properties of ENVISAT ASAR and QuikSCAT Surface Winds in the North Sea. Remote Sensing, 5(11), 6096-6115. https://doi.org/10.3390/rs5116096

Kennedy, J.J. (2014), A review of uncertainty in in situ measurements and data sets of sea surface temperature: IN SITU SST UNCERTAINTY, Rev. Geophys., 52, pp. 1-32, doi:10.1002/2013RG000434

Nielsen-Englyst, P., Høyer, J.L., Karagali, I., Kolbe, W.M., Tonboe, R.T., and Toudal Pedersen, L.L. (2024), Impact of microwave observations on the estimation of Arctic sea surface temperatures, Remote Sensing of Environment, 301, 113949, doi:10.1016/j.rse.2023.113949.

Nielsen-Englyst, P., Høyer, J.L., Kolbe, W.M., Dybkjær, G., Lavergne, T., Tonboe, R.T., Skarpalezos, S., and Karagali, I. (2023), A combined sea and sea-ice surface temperature climate dataset of the Arctic, 1982–2021, Remote Sensing of Environment, 284, 113331, doi:10.1016/j.rse.2022.113331.

Nielsen-Englyst, P., Høyer, J.L., Toudal Pedersen, L.L. Gentemann, C., Alerskans, E., Block, T. and Donlon, C. (2018), Optimal estimation of sea surface temperature from AMSR-E, Remote Sens., 10, p. 229, doi:10.3390/rs10020229

Ohring, G., Wielicki, B., Spencer, R., Emery, B., and Datla, R., (2005), Satellite instrument calibration for measuring global climate change: report of a workshop. Bull. Amer. Meteor. Soc., 86, pp. 1303-1314, doi:10.1175/BAMS-86-9-130.

Thomson, R.E. and Emery, W.J. (2014), Data Analysis Methods in Physical Oceanography, Chapter 4: The spatial analysis of data fields, pp. 313-424, Elsevier, doi:10.1016/C2010-0-66362-0.

Vazquez-Cuervo, J., Castro, S. L., Steele, M., Gentemann, C., Gomez-Valdes, J., and Tang, W. (2022). Comparison of GHRSST SST Analysis in the Arctic Ocean and Alaskan Coastal Waters Using Saildrones. Remote Sensing, 14(3), 692. https://doi.org/10.3390/rs14030692

WMO (2022), The 2022 GCOS ECVs Requirements, GCOS-245, Geneva 2022, p 244, *https://library.wmo.int/idurl/4/58111*

Copernicus Climate Change Service

ECMWF – Robert-Schuman-Platz 3, 53175 Bonn, Germany

Contact: https://support.ecmwf.int/